TALLINNA TEHNIKAÜLIKOOL
TALLINN UNIVERSITY OF TECHNOLOGY

Department of Materials and Environmental Technology

FULLY ELECTROSPUN FLEXIBLE POLY(STYRENE-CO-ACRYLONITRILE) SUPERCAPACITOR ELECTRODES

TÄIELIKULT ELEKTROKEDRATUD PAINDUVAD STÜREEN-AKRÜÜLNITRIILKOPOLÜMEERIST SUPERKONDENSAATORI ELEKTROODID

MASTER THESIS

Student: Agnes Kuus

Student code: KVEM163220

Supervisor: Dr Viktoria Vassiljeva, engineer

Tallinn, 2018

AUTHOR'S DECLARATION

Hereby I declare that I have written this thesis independently.
No academic degree has been applied for based on this material. All works, major viewpoints and data of the other authors used in this thesis have been referenced.

".....” 2018

Author: .....
/signature /

Thesis is in accordance with terms and requirements

".....” 2018

Supervisor: .....
/signature/

Accepted for defence

".....”.....2018 .

Chairman of theses defence commission: .....
/name and signature/

Department of Materials and Environmental Technology

THESIS TASK

Student: Agnes Kuus, KVEM163220

Study programme: Technology of Wood, Plastic and Textiles, KVEM12/15

Main speciality: Technology of plastics and textiles

Supervisor: Dr Viktoria Vassiljeva, engineer, +37256260175

Thesis topic:

(in English) Preparing novel flexible electrospun supercapacitor electrodes, their characterisation and comparison with other flexible EDLC electrodes described in scientific literature

(in Estonian) Uudsete painduvate elektrokedratud superkondensaatorite elektroodide valmistamine, nende karakteriseerimine ja võrdlus teaduskirjanduses kirjeldatud teiste painduvate superkondensaatorite elektroodidega

Thesis main objectives:

1. Finding best method for the dispersion of the carbonous additives.
2. Production of supercapacitor electrodes via electrospinning technique.
3. Evaluation of the properties of prepared dispersions and electrospun supercapacitor electrodes.

Thesis tasks and time schedule:

No	Task description	Deadline
1.	Preparing dispersions and producing supercapacitor electrodes via electrospinning	30.01.2018
2.	Characterising solutions and electrospun electrodes	30.03.2018
3.	Writing of thesis	09.05.2018

Language: English **Deadline for submission of thesis:** "....."....201….a

Student: Agnes Kuus ..... "....."....201….a
/signature/

Supervisor: Viktoria Vassiljeva ..... "....."....201….a
/signature/

CONTENTS

PREFACE

This thesis was part of the project “Fully electrospun durable electrode and electrochemical double-layer capacitor for high frequency applications” in cooperation with Tallinn University of Technology (TTU), European Space Agency and Skeleton Technologies Ltd. The major part of thesis work was done in the Laboratory of Polymers and Textile Technology in TTU by the author of the thesis. Scanning electron microscopy images of membranes and carbonous additives were done by Dr V. Mikli, electrochemical cell preparation was conducted by Dr E. Tarasova, cyclic voltammetry tests on electrochemical cells were performed by PhD student S. Malmberg and Skeleton Technologies Ltd and BET analysis was conducted by Dr M. Uibo.

I wish to express my deep gratitude to my supervisor Dr Viktoria Vassiljeva for the knowledge and experience she shared with me, for always finding new opportunities to improve the content of my thesis and for motivating me to contribute the maximum of myself. I also want to thank Dr E. Tarasova, Dr M. Uibo, Dr V. Mikli, and S. Malmberg for conducting the abovementioned characterisations of electrospun membranes, and Dr I. Krasnou for always encouraging me to find the reasons behind my results.

The aim of this thesis was to produce novel electrospun poly(styrene-co-acrylonitrile) and carbide-derived carbon composite membranes which could be used as flexible supercapacitor electrodes. The electrospinning solutions were prepared using two different methods and they were characterised by conductivity and rheology measurements. The electrospun membranes were characterised by different techniques to study their morphology, conductivity, mechanical properties and electrochemical properties to evaluate their potential use as supercapacitor electrodes. The prepared composite membranes were flexible, foldable and twistable, with a high gravimetric capacitance and a good tensile strength.

Keywords: poly(styrene-co-acrylonitrile), electrospinning, carbide-derived carbon, supercapacitor electrode, master thesis

List of abbreviations

$BMImBF_4$	1-butyl-3-methylimidazolium tetrafluoroborate
BMImCl	1-butyl-3-methylimidazolium chloride
CA	cellulose acetate
CB	carbon black
CDC	carbide-derived carbon
CDC-SiC	silicon carbide derived carbon
CDC-TiC	titanium carbide derived carbon
CNF	carbon nanofiber
CNT	carbon nanotube
CV	cyclic voltammetry
DCE	1,2-dichloroethane
DLS	dynamic light scattering
DMF	N,N-dimethylformamide
DMSO	dimethyl sulfoxide
EDLC	electrochemical double-layer capacitor
EES	electrical energy storage
$EMImBF_4$	1-ethyl-3-methylimidazolium tetrafluoroborate
IL	ionic liquid
M1	method 1
M2	method 2
PAN	polyacrylonitrile
SAN	poly(styrene-co-acrylonitrile)
SEM	scanning electron microscopy
SiC	silicon carbide
SSA	specific surface area
TEMA/AN	triethylmethylammonium tetrafluoroborate in acetonitrile
TiC	titanium carbide
VC	vanadium carbide

INTRODUCTION

Supercapacitors are energy storage devices used for applications where high power density and good energy density are needed, for example for breaking energy storage in cars, for emergency doors on the planes or for short-term power backups [1]. In the future, they could also replace batteries in mobile power supply applications to obtain very rapid charging speeds of devices, or they could make possible the reasonable storage of electric energy produced by windmills and solar panels. Further, if these supercapacitors are also flexible and have a good tensile strength, they could be used in wearable and portable electronics. However, supercapacitors which can store a higher amount of energy, have to be developed first to implement their full potential in these applications. [2, 3] As the electrode material is a key component for increasing the performance of supercapacitors, the research into developing the supercapacitor electrodes has grown exponentially in the last 20 years, and also promising results have been achieved. [3]

A lot of published studies are dedicated to preparing nanoporous carbons (e.g activated carbons or carbide-derived carbons) to obtain higher surface areas and higher capacitance. However, these carbon particles are usually manufactured into a rigid electrode by bonding the carbon particles with a binder substance. [3] On the other hand, free-standing and binder-free electrodes with outstanding flexibility, good electrochemical performance and light weight are crucial for implementing the flexible supercapacitors in wearable consumer electronics or portable electronics like roll-up displays and electronic paper. [4]

Such free-standing and flexible electrodes could be produced by electrospinning method. When compared to other available flexible membrane preparing methods, electrospinning is a simple and easily scalable method that allows producing intrinsically capacitive membranes. Further, electrospinning enables to produce fibers with sub-micrometre diameters, therefore enabling to increase the specific surface area (SSA) of the membrane, which is crucial for obtaining supercapacitor electrodes with a high capacitance. [5] The electrospinning technique can be applied to carbonous additive containing polymer dispersions to produce carbon-polymer composite fibrous membranes that possess the critical properties (flexibility, good electrochemical performance, sufficient tensile strength, light weight and freedom from binders) needed for flexible supercapacitor electrodes [6].

Inspired by the challenge of producing flexible supercapacitor electrodes with good performance, the aim of this work was to develop novel fully electrospun poly(styrene-co-acrylonitrile) (SAN) and carbide-derived carbon (CDC) composite material with a potential use as free-standing and flexible supercapacitor electrodes.

To achieve this aim, the objectives of the study were:

1. Finding the best method for the dispersion of carbonous additives by comparing two different dispersion preparation methods.
2. Producing supercapacitor electrodes by electrospinning the SAN and CDC dispersions.
3. Evaluating two properties of prepared dispersions, conductivity and rheology, to compare the different dispersions, different dispersion preparation methods and to study their effect on membrane properties.
4. Studying different properties of the electrospun membranes, including morphology, conductivity, porosity, specific surface area, tensile strength and specific capacitance of membranes, and studying correlations between these properties.
5. Evaluating the application of prepared membranes as supercapacitor electrodes and comparing them to other flexible supercapacitor electrodes described in scientific literature.

1 LITERATURE REVIEW

1.1 Supercapacitors

The electricity generation is changing rapidly across the world due to the need to reduce the use of fossil fuels and reduce the greenhouse gas emissions. Thus, the renewable energy sources are increasingly used. As most of the renewable energy sources are intermittent in their nature, the electrical energy must be stored to maintain the energy generation and load balance. This can be done by using an electrical energy storage (EES) technology, which converts the electrical energy to a storable form, reserves it, and later enables to convert it back into electrical energy. Supercapacitors are a type of EES devices that can store the electric energy in the form of static charge. Supercapacitors have been used for example to smooth the fast wind-induced power variations and can be also combined with fuel cells and batteries for even wider EES applications. [7]

Supercapacitors have a unique combination of high power capability and good energy density, which situates them in the functional position between conventional capacitors and batteries (Figure 1.1) [8, 9]. In addition, the shelf life and cycle life of the supercapacitors are much higher than those of batteries because there are no or are very small chemical charge transfer reactions involved. The supercapacitors have also a high efficiency discharge in which only 5% of the energy is dissipated in heat. Batteries with the same efficient discharge would have a much lower power capability than the supercapacitors have. Other advantages of the supercapacitors include fast charge propagation and charge-discharge processes which take only seconds, very long cycle life, minimal maintenance requirement, low self-discharging rate, environmental-friendliness and wide operation temperature range. These qualities have created much interest in the supercapacitors for a wide range of applications, including for example portable electronics like cell phones, memory backup systems and hybrid electric vehicles, where fast charging is a valuable quality. [9-12]

Research into supercapacitors is divided into two areas: pseudocapacitors and electrochemical double-layer capacitors (EDLCs). In a pseudocapacitor the charge storage is based on a redox process while in an ideal EDLC the charge is stored within the electrochemical double-layer at the electrolyte and solid electrode interface. [8, 10] As a result of their working mechanism,

pseudocapacitors exhibit high energy density but low power density, while EDLCs possess the opposite performance [5]. In the present work, only EDLC supercapacitors are considered.

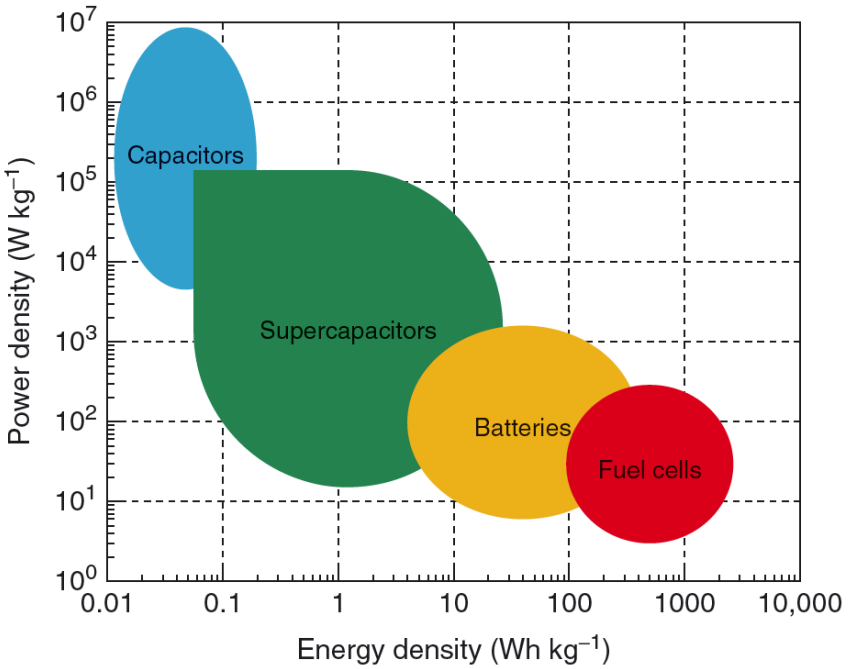

Figure 1.1. Power density vs energy density values for various energy storage and conversion devices [13]

1.1.1 Basic design of supercapacitors

A supercapacitor unit cell is constructed similarly to a battery as there are two electrodes immersed in an electrolyte which are isolated from electrical contact by a porous ion permeable separator [8, 12]. This allows ionic current to flow between the electrodes while preventing electronic current from discharging the cell [12]. When a voltage is applied to the capacitor, positive and negative ionic charges within the electrolyte accumulate near the solid electrode's surface and compensate for the electronic charge at the electrode surface. The concentration of the electrolyte and the size of the ions determine the thickness of the double-layer which in turn determines the capacitance of EDLC. For concentrated electrolytes, the thickness of the double-layer is in the order of 0,5-1 nm. [9, 13]

Current collectors of metal foil are used to conduct electrical current from each electrode [14]. The current collectors are needed to overcome the electrode material's inadequate conductivity and to dissipate heat generated within the cell. Aluminium foil is the most commonly used current collector. [13] Depending on the desired size and voltage of the supercapacitor, multiple repeating

unit cells can be constructed into a supercapacitor module [14]. Scheme of an electrochemical double-layer capacitor is shown in Figure 1.2.

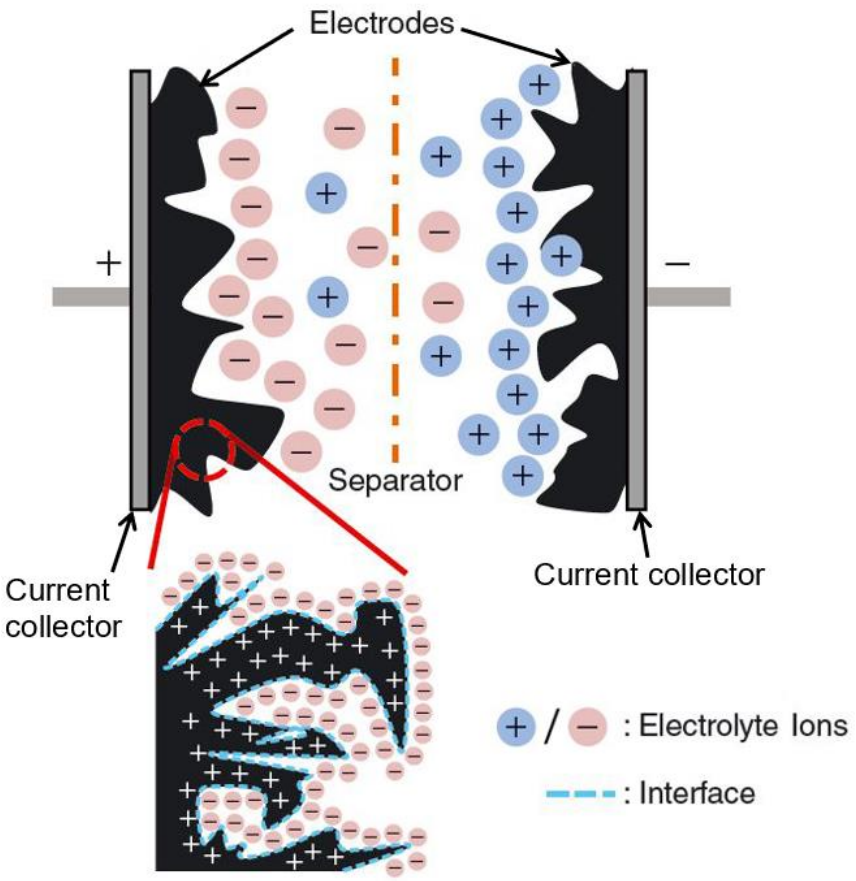

Figure 1.2. Single-cell electrochemical double-layer supercapacitor (in a charged state), adapted from [13]

There are three types of electrolytes used in supercapacitors: aqueous, organic, and ionic liquids. Electrolytes affect the cell's operating voltage window and therefore the energy density of the cell which is proportional to the square of the voltage window. Commercially available supercapacitors employ usually organic electrolytes because of their wide operating voltage window (0 to 2,7 V), compared to the narrow voltage window of aqueous electrolytes (0 to 1,2 V). Although ionic liquids have an even wider operating voltage window, their usage is restricted by inadequate ionic conductivity when compared to the other two types of electrolytes. [13]

The capacitance of the EDLC is determined by the electrode material and thus can be increased by using porous materials with extremely large internal effective surface as electrodes [9]. A widely used electrode material in EDLCs is a type of abundant and inexpensive carbon known as activated carbon. Activated carbons can exhibit specific capacitance values up to 100-120 $F \cdot g^{-1}$ in organic

electrolytes. [13] Potentially, for a surface area of 1000 $m^2 \cdot g^{-1}$, the electrode material could have a capacitance of 150-300 $F \cdot g^{-1}$. However, these potential capacitance values are usually not achieved, because a relatively large fraction of the surface area is in pores that cannot be accessed by the electrolyte ions. This inaccessibility is more pronounced in the case of organic electrolytes which have much larger ions than aqueous electrolytes. [10]

1.1.2 Supercapacitor electrodes

The electrode material of EDLC should have following properties: a large surface area and high porosity, good surface wettability towards the electrolyte, good electrical conductivity, long cycle stability, easy manipulation of morphology (e.g. the size and distribution of pores, particle dimensions) and thermodynamic stability for a wide operational potential window. Carbon materials are widely accepted for EDLC electrodes as they possess several of these characteristics. Furthermore, they are also abundant, light-weight and of moderate cost. Modified carbons used for EDLC electrodes include activated carbons, carbide-derived carbons (CDCs), onion-like carbons, carbon nanotubes (CNTs), carbon aerogels and graphene. [11, 13] These carbon particles are usually manufactured into a rigid electrode by bonding the carbon particles with a binder substance [3].

Activated carbons are the most commonly used electrode materials in EDLCs due to lower cost and higher surface area than other carbon materials. However, their applications are still restricted due to limited energy storage and rate capability. Activated carbons have a complex porous structure composed of micropores, mesopores, and macropores. The control of the pore structure and pore size distribution to be narrow enough to maximise the pore accessibility to the electrolyte ions, is still challenging. In addition to tailoring the pore structure, surface modification (e.g. exfoliation, surface activation, N-doping or S-doping) of activated carbons would be beneficial in aiding to increase the capacitance of carbon-based materials and thereby widen the application of carbon electrodes. [1, 5, 15]

1.1.3 Pore size and capacitance

Initially the research on activated carbons was directed towards increasing the pore volume by developing high specific surface area and refining the activation process. However, it has been now

shown, that there is no linear relationship between the specific surface area and the capacitance. Several studies have reported an important capacitive contribution from micropores (<2 nm pores). Experiments using CDCs as the active material provided evidence that capacitance increased from pores smaller than the solvated electrolyte ion size, indicating that a partial or complete removal of their solvation shell was allowing the electrolyte ions to access the micropores. The gravimetric and volumetric capacitances obtained with CDC were 50% and 80% higher than for conventional activated carbons. Furthermore, a study with a solvent-free electrolyte showed that the maximum capacitance was obtained when the electrolyte ion size and electrode material's pore size were equal (0,7 nm in the given study), demonstrating that a single ion per pore produced the maximum capacitance. [16, 17]

At the same time, nanopores with even smaller diameter than the electrolyte ion size may not be accessible to the electrolyte ions as the ions are simply too large to enter into the nanopores. Therefore the surface area of these non-accessible nanopores will not contribute to the total double-layer capacitance of the electrode material. [18] In addition to matching the pore size of carbon to the size of the electrolyte ions to obtain the maximum energy density, the carbon should also contain mesopores (2-50 nm pores). Mesopores are necessary to provide the transport channels which allow electrolyte ions to access the micropores. Allowing the rapid ion transport by having either large mesopores or straight small mesopores is needed to obtain the high power density of the supercapacitor. [19, 20] Thus, an ideal supercapacitor electrode material should contain large amount of micropores with sizes similar to those of the electrolyte ions, no micropores smaller than that, and a fair amount of mesopores for the ion transport to obtain both good energy density and high power density.

1.1.4 Performance of the electrode materials

The abovementioned energy density [$W \cdot h \cdot kg^{-1}$] and power density [$W \cdot kg^{-1}$] are the key parameters of the supercapacitor at the packaged EDLC cell level. However, these parameters are not applicable for material level performance reporting since they depend also on package specific parameters like cell architecture and mass of the other cell components. Thus, to compare the performance of different electrode materials, the most important metric is their specific capacitance [$F \cdot g^{-1}$], which is the capacitance per unit mass of the active material. [14]

A test fixture configuration that closely mimics the EDLC's unit cell configuration matches also the performance of a packaged cell more closely. Both two-electrode and three-electrode test fixtures are commonly used in electrochemical research. However, the three-electrode test fixture consists of a working electrode, a reference electrode, and a counter electrode which can result in values double those of the two-electrode cell. This heightened sensitivity of the three-electrode configuration can lead to large errors when projecting the energy storage capability of an electrode material for supercapacitor use. A two-electrode test cell mimics the physical configuration, internal voltages and charge transfer that occurs in the packaged supercapacitor and therefore provides the best indication of an electrode material's performance. [14]

The electrochemical results are also influenced by the mass of the active material and by the thickness of the electrodes. Extremely thin electrodes and electrodes that contain only a very small amount of active material can lead to an over-statement of the material's performance. For reliable measurements, the mass of the active material should be on the order of 10 mg or more and the thickness of the electrode should be between 10 µm to several hundred micrometres. Furthermore, the electrode material's performance depends also on the used electrolyte. An aqueous electrolyte will usually yield higher specific capacitance values and does not indicate its performance with an organic or ionic liquid electrolyte. [14]

1.1.5 Methods for producing flexible electrodes

Researchers in EES field have lately focused on developing flexible supercapacitors with good electrochemical and mechanical performance. High power density, superior stability, low cost, high safety and the integration of flexibility in supercapacitors are of great importance for powering various flexible electronics. Flexible and wearable supercapacitors hold also great promise as new energy storage devices for wearable electronics. [5]

The simplest route to obtain flexible supercapacitors would be to coat flexible films or fabrics with active and conductive materials by for example repeated dip-coating method or by coating slurries to the film or fabric assisted with a blade or roller to ensure uniform thickness. However, in most cases, the active carbon material can be easily peeled off from the current collector when the supercapacitors are bent, twisted or stretched. [5, 21]

The active materials have been also grown in-situ on textile or film surfaces [21]. For example, electrodeposition method has been widely used for producing flexible pseudocapacitive electrodes from conducting polymers and transition metal oxides. However, electrodeposition usually leads to a dense structure which impedes the infiltration between the polymer and electrolyte and thus lowers the capacitance. [5] To achieve better performance, several fabrication methods have been used together. For example, Lee *et al*. deposited MnO_2 micronodules onto the surface of a carbon fabric by electrodeposition, then a partially carbonized polypyrrole polymer was coated onto the MnO_2 surface through vapour deposition polymerization. They achieved a high volumetric specific capacitance 59,5 $F \cdot cm^{-3}$ and this is one of the best electrochemical performances of supercapacitor fabrics in the literature. [21]

Developing flexible fabrics with intrinsic energy storage capability is regarded as a more promising strategy and this can be done using various spinning methods. The spinning methods can potentially eliminate the interfacial adhesion problems between electrode materials and supporting flexible substrates. Most importantly, these spinning methods can be also well scaled to the industry level. [21] Conventional wet spinning or dry spinning methods enable to produce fibers with smallest diameters in only micrometre range, however, sub-micron fibers or nanofibers would be desirable for fabricating supercapacitor electrodes due to larger surface-to-volume ratio. Electrospinning method has been also used to produce supercapacitor electrodes. Electrospinning provides a way to produce sub-micron fibers that do not suffer from the dense structure that is accompanied with electrodeposition method and from delamination of active materials from a substrate which is accompanied with coating methods. [5] The practicality of electrospinning has been also greatly improved recently due to advances in mass production scalability, resulting in higher production rate and therefore lower cost materials [22]. In the next chapter, electrospinning method is reviewed in more depth and producing EDLC electrodes by electrospinning is discussed.

1.2 Electrospinning

Electrospinning is a simple and scalable technique that uses electrostatic force to form high aspect ratio nanofibers with controllable diameter. Electrospun nanofibers combine several physical properties that make them attractive for supercapacitor electrode preparation, for example large specific surface area, high degree of flexibility, high mechanical strength, strain-induced electronic

properties and tailorable pore distribution. [23] A vast range of materials can be electrospun into continuous nanofibers. Although electrospinning is one of the best known methods to produce polymer fibers, also composites, semiconductors and ceramics can be electrospun. [24, 25]

1.2.1 Electrospinning process

Electrospinning technique uses high electric potentials to overcome the surface tension of the solution. In the process, a high positive voltage, typically 10-30 kV in the case of a single-needle setup, is applied to a polymer solution which is usually contained in a syringe, with respect to a grounded collector (Figure 1.3A). When the voltage is applied, ions present in the solution start to accumulate at the air-solution interface. [25] The electrostatic repulsion between the charged ions favours the creation of a jet, while the surface tension of the solution favours a spherical shape with smaller surface area per unit mass. Once the electric potential of the surface is increased to a sufficiently high value (a threshold value), the electrostatic repulsion overcomes the surface tension of the solution and consequently, a solution jet erupts. The solution jet travels towards the collector, experiencing an elongation with a strong diameter reduction during the flight. At the same time, the solvent evaporates, leaving behind a charged polymer fiber. Finally, the fibers are collected on the collector as a nonwoven membrane. [25-27]

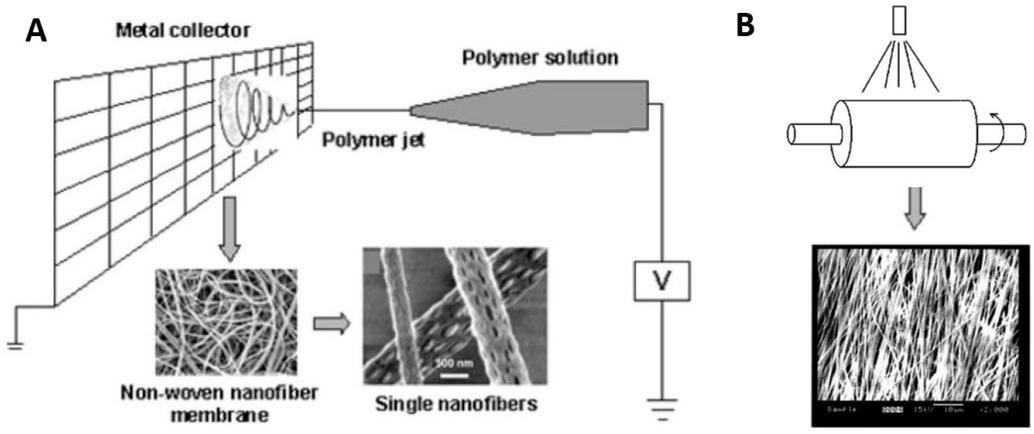

Figure 1.3. A – schematic of the electrospinning process with a static plate collector and an image of randomly oriented fibers. B – a rotating cylinder collector with an image of aligned polymer fibers, adapted from [27]

The fluid jet is characterised by three different regions: a droplet at the tip of the syringe, a stable straight region close to the syringe tip with length in the order of 1 cm, and a region of unstable

bending motion with the jet moving laterally and forming series of coils towards the collector, where fibers are collected. [25]

The simplest collector type is a static plate collector onto which fibers are deposited randomly. However, many applications, including supercapacitor electrodes, favour a membrane where fibers are aligned along a preferential direction. There are several strategies that have been proposed to obtain aligned fibers, for example using a parallel electrode collector, a rapidly oscillating grounded frame or a rotating cylinder (Figure 1.3B) instead of the simple plate collector. The relation between the linear speed of the rotating collector surface and the jet deposition is of critical importance for an effective control over the fiber alignment. When the linear speed of the collector surface matches the speed of jet depositions, the fibers are collected on the cylinder surface tightly in a circumferential manner, resulting in a fair alignment. If the surface speed of the collector is slower than that, randomly deposited fibers will be collected. However, there is also an upper limit to the rotating speed above which the fiber jet will be broken and continuous fibers cannot be collected. [25]

1.2.2 Electrospinning parameters

The formation of nanofibers and their properties are determined by many electrospinning parameters. These parameters can be divided into three categories: solution parameters, process parameters, and ambient conditions [28] and can be seen in more detail in Table 1.1. The structure of the resulting fibrous membrane can be tuned by carefully modifying these parameters. [29] When polymers are electrospun into nanofibers, there are three targets that are strived to achieve: 1) the fiber diameters are consistent and controllable, 2) the fiber surface is without defects or the defects are controllable, and 3) continuity of the single nanofibers can be achieved [27].

Table 1.1. Electrospinning parameters that influence the fiber formation and morphology

Type	Parameter	Impact on electrospun fiber characteristics
Solution parameters	Solution viscosity, concentration and molecular weight of polymer	Solution viscosity is the most significant parameter influencing the fiber diameter. Higher solution viscosity yields fibers with larger diameter. The solution viscosity is influenced by the solution concentration and the molecular weight of the polymer. The increase in fiber diameter has been found to be proportional to the cube of the polymer concentration. [27, 28, 30]

Table 1.1 (continued)

Type	Parameter	Impact on electrospun fiber characteristics
Solution parameters	Solution viscosity, concentration and molecular weight of polymer	Solution viscosity also affects strongly the fiber continuity and morphology. At low viscosity, only droplets of polymer solution (electrospray) is collected. An increase in the solution concentration or in the molecular weight of polymer and thus an increase in viscosity yields beaded fibers. A further increase will result in fibers with fewer beads or even completely smooth fibers. [28, 31] Too high solution viscosity can obstruct pumping the solution out of the syringe and the solution will also dry faster on the needle tip, potentially leading to clogging of the needle. Above a critical solution viscosity, no continuous fibers can be obtained. [32]
	Solution conductivity	Increase in electric conductivity of the solution results in the decrease of fiber diameter as the bending instability increases and the solution jet travels a longer distance. Highly conductive solutions can also yield fibers with broader diameter distribution. [31] The increased conductivity can reduce or eliminate the bead formation and it favours the formation of uniform smooth fibers [31, 33]. However, if the solution conductivity is increased over a certain point, the fiber diameters can increase due to the delayed onset of the bending instability and therefore shortened fiber stretching process [34].
Process parameters	Distance between the tip of the needle and collector	The distance affects the fiber morphology, although the effect is smaller than with other parameters. A minimum distance is required for sufficient solvent evaporation before the fibers reach the collector and shorter distances can result in bead formation. Longer distance has yielded smaller fiber diameters and less beads, as the jet elongates more and the solvent has more time to evaporate before the fibers reach the collector. [28, 31]
	Inner diameter of needle	A needle with too small diameter can become clogged. The larger the needle diameter, the lower voltage is needed for electrospinning which will result in thicker fibers. The smaller the needle diameter, the greater electrostatic force is needed to overcome the surface tension and consequently, thinner fibers are formed. [32]

Table 1.1 (continued)

Type	Parameter	Impact on electrospun fiber characteristics
Ambient parameters	Humidity	A study on polystyrene fibers showed that high humidity can result in circular pores on the fibers [31]. Humidity can also cause changes in the fiber diameter by controlling the solidification process of the fluid jet, however, this phenomenon is dependent on the chemical nature of the polymer [35]. Very low humidity can cause a volatile solvent to evaporate too rapidly which can lead to clogging of the needle tip [31].
	Temperature	Increase in temperature increases the solvent evaporation rate and at the same time decreases the solution viscosity. Both of these mechanisms lead to decrease in fiber diameter. [31, 35]

In addition to the parameters presented in Table 1.1, the solution components (solvent or solvent mixtures, fillers, conductive additives, polymer or polymer mixtures) have also a significant role in determining the electrospun fiber morphology and properties [27, 35].

1.2.3 The role of solvents and additives in electrospinning

Electrospinning solution in its simplest form consists of a polymer dissolved in a solvent. However, often the mechanical, electrical, thermal, rheological and optical properties of electrospun fibers need improvement for special applications. Depending on the application, different fillers and additives can be dispersed or dissolved in the solution to enhance these properties. [32] Further, different solvents or solvents mixtures can be used to drastically change the morphology and properties of fibers, for example their diameter or porosity [35].

Solvent. The selection of the solvent is one of the key factors for achieving smooth and bead-less electrospun fibers. There are two important things that should be kept in mind when selecting a solvent: the chosen solvent should be able to completely dissolve the polymer, and secondly, the solvent should have a moderate boiling point. The boiling point influences the volatility of a solvent and generally, volatile solvents are preferred in electrospinning due to their higher evaporation rate. Most of the solvent should evaporate during the fluid jet's travelling from the syringe to the collector. However, highly volatile solvents are usually avoided because their high evaporation rates cause the drying of the jet at the needle tip, which can block the needle and therefore hinder or break off the electrospinning process. [35] The dipole-moment and conductivity of the solvent

are also of importance. Solutions containing solvents with better conductivity and dipole-moment values are more feasibly and easily electrospun, a study observed. [36]

A polymer dissolved in different solvents can show dramatic differences in electrospun fiber morphology [37]. For example, in a study with cellulose acetate (CA), when CA was electrospun in acetone solvent or in dimethylacetamide solvent, beaded fibers were obtained. However, if CA was electrospun in acetone and dimethylacetamide solvents mixture with ratio 2:1, completely bead-free smooth fibers were produced. [27] Furthermore, the porosity of fibers can be changed with solvents. For instance, highly porous nanofibers can be obtained when a polymer is dissolved in two solvents, one of which acts as a non-solvent. The different evaporation rates of the solvent and non-solvent result in phase separation which in turn results in the fabrication of highly porous electrospun nanofibers. [35]

Additive. The use of additive in the electrospinning solution may affect different properties. Charge carriers such as salts or conductive additive particles influence the conductivity of the solution and they may promote two phenomena having opposite effects on fibre formation. Firstly, they may increase flow rate, which can lead to larger fibers. Secondly, they may increase net charge density, which leads to formation of bead-free and thinner fibers. [38] In addition to charge carrier additives, also magnetic nanoparticles like FePt, mechanical strength increasing nanoparticles like carbon nanotubes and even viruses and bacteria have been added to polymer solutions and successfully electrospun [37].

In addition to changing the properties of electrospun fibers and therefore widening their applications, additives can also influence the electrospinning process. Fillers and additives may interact with the solvent, with polymer or with both which can as a result change the electrospinnability of the solution. The additive particles can change the solution viscosity which also results in the change of the fiber diameter. A higher viscosity due to additive particles can further lead to clogging of the needle. For tertiary systems, the optimization of process parameters is even more challenging than for binary systems composed of only a polymer and a solvent. [38]

1.2.4 Producing EDLC electrodes by electrospinning

Electrospinning has been considered as a promising method for the design and fabrication of materials for flexible EES devices, including supercapacitors. These fibers can be mixed with active

materials to produce fabrics that can be assembled into completely flexible and lightweight supercapacitors. [39]

More than 70% of scientific publications on electrospun fibers for supercapacitor electrodes use carbon-based fibers. Most of the carbon nanofibers (CNFs) prepared by electrospinning are prepared from polyacrylonitrile (PAN) solutions in dimethylformamide (DMF). These electrospun PAN fibers are carbonized by annealing under a neutral atmosphere and finally activated by annealing under an oxidative atmosphere. The activation process allows the development of the micro- and mesopores leading to a drastic increase in the surface area and therefore to the increase in capacitance of the material. With this method, specific surface areas up to 1200 $m^2 \cdot g^{-1}$ have been achieved. Flexible and porous CNFs have been also obtained from electrospinning a mixture of titanium butoxide, furfuryl alcohol and polyvinyl pyrrolidone polymer in DMF and acetic acid solvents, the obtained nanofelts were dry chlorinated at temperatures up to 1000^oC to obtain porous and flexible carbon-derived carbon nanofibers with a specific capacitance of 135 $F \cdot g^{-1}$. [38-40]

Another option for EDLC electrode production is to disperse high surface area carbon powder in a polymer solution and then electrospin the obtained dispersion. For example, Lust *et al*. electrospun a mixture of activated carbon in a polyvinylidene fluoride polymer solution directly onto the previously electrospun separator and produced half-cells with specific capacitance up to 120 $F \cdot g^{-1}$ at 1 $mV \cdot s^{-1}$. They also found that EDLCs based on these electrospun composite electrodes were able to deliver much faster and higher power at applied constant energy than the EDLCs based on the electrodes prepared by the traditional roll-pressed method. [6, 39]

Styrene and acrylonitrile copolymer SAN was chosen in this work as the polymer for producing the electrospun supercapacitor electrodes. The electrospinning of SAN will be discussed in more depth in the next chapter.

1.2.5 Electrospinning of SAN

Poly(styrene-co-acrylonitrile) (SAN) is a copolymer prepared from styrene and acrylonitrile monomers (Figure 1.4) with acrylonitrile content usually between 20 to 30%. The acrylonitrile content influences the mechanical properties of SAN, higher acrylonitrile content increases the tensile strength and elongation of SAN. SAN copolymers have also improved heat and chemical resistance over pure polystyrene. [41] Furthermore, as potentially very thin and porous SAN fibers

can be produced by electrospinning [42, 43], their application in supercapacitor electrode preparation would be very beneficial. The small diameter and porosity of fibers can aid in increasing the specific surface area of the electrode, and the open pores in fibers can allow the electrolyte ions to access the pores of carbonous additives, which could be dispersed inside the fibers. All these properties together could lead to supercapacitor electrodes with increased capacitance that are at the same time also flexible. Due to these reasons the SAN polymer was chosen in this work for EDLC electrode preparation.

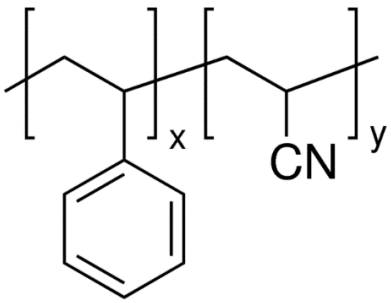

Figure 1.4 Chemical structure of poly(styrene-co-acrylonitrile), where x is styrene and y is acrylonitrile part [44]

SAN has been successfully electrospun in dimethyl sulfoxide (DMSO), N,N-dimethyl formamide (DMF) and in 1,2-dichloroethane (DCE) solvents [30, 42, 45]. When SAN was electrospun in DMSO, the change from beaded fibers to smooth fibers began at a concentration of 12%, the average diameter at the same concentration was 267 nm. When the solution concentration was increased to 15%, uniform bead-free fibers with 470 nm diameter were formed due to the higher number of entanglements. [30] A study also demonstrated, that SAN fibers with porous structure can be obtained when SAN is electrospun in DMSO [43].

Very thin fibers have been obtained when SAN was electrospun in DMF. In this case, 15% concentration was found to be the critical entanglement concentration at which a mixture of microbeads and smooth fibers were produced with an average fiber diameter of 138 nm. When the concentration of SAN in DMF was increased to 20% and therefore above the critical entanglement concentration, very few beads were obtained compared to lower concentration solutions and the average fiber diameter increased from 138 nm to around 300 nm. [42]

Due to the lower boiling point of DCE, electrospinning of SAN in DCE was more difficult as the needle became clogged both at lower concentration (10%) and higher concentration (20%), however, it was possible to electrospin SAN in DCE at concentrations between those and was successfully

electrospun at 13% and 17%. At 13% concentration, the obtained average fiber diameter was 2 µm but could be reduced down to 275 nm when 20% of ionic liquid 1-butyl-3-methylimidazolium chloride (BMImCl) was added to the solution. [45]

1.3 Carbonous materials in EDLCs

Several different carbonous materials are used for EDLC electrode preparation, such as activated carbons, graphene, CDCs and CNTs. In the following subchapters, two carbonous additives which were used in this work, are discussed in more depth.

1.3.1 Carbide-derived carbon

Carbide-derived carbons (CDCs) are a type of carbons that are very attractive for use in the supercapacitor electrodes as the active material, due to the controllability of their pore size distribution and specific surface area. CDCs are synthesised by the extraction of metals from metal carbides (e.g. TiC, SiC, VC or ZrC), resulting in a carbon termed as carbide-derived carbon. The extraction of the metal can be accomplished through several ways, but high-temperature chlorine treatment of carbides (Eq 1.1) has become the most commonly used method. The morphology and porosity of the carbon structure is dependent on the originating carbide form and this allows a pore size control on the sub-nanometre level. [19]

$$SiC_{(s)} + 2\ Cl_{2(g)} \rightarrow SiCl_{4(g)} + C_{(s)} \quad (1.1)$$

One key feature of CDC is the shape preservation. When a metal carbide of desired shape is converted to carbon, the general shape and volume of the original carbide is maintained. The porosity created within CDC is a function of variables, including initial carbide chemistry and porosity, processing parameters and post-chlorine treatment. Using appropriate processing conditions, it is possible to create a very uniform and controlled pore structure within CDC when compared to other carbon synthesis methods. In addition to the porosity developed during chlorine treatment, there are treatments that may be applied to further develop the pore structure. In this case, usually an agent (O_2, CO_2, or KOH) is used to remove carbon atoms, resulting in an increase of the average pore size and pore volume. This allows to create more transport pores which is favourable as in microporous CDC there is typically a deficiency of transport pores, leading to decreased power characteristics of the supercapacitor. [19, 20]

Many CDCs have been tested in supercapacitors, including TiC and SiC derived CDCs in various electrolytes. The high surface area and micropores in CDCs have resulted in high specific capacitances in organic electrolytes and the energy and power densities achieved are some of the highest reported in both organic and aqueous electrolytes. Therefore, CDCs show significant promise for improving the performance of commercial EDLCs, which currently use mostly activated carbons, and thus producing high-performance supercapacitors. [19]

Among all the carbides, titanium carbide (TiC) is one of the most widely used precursors for CDCs [46]. It is commonly observed that the TiC derived amorphous carbon has a BET surface area around 1400 $m^2 \cdot g^{-1}$ and can be increased up to 1900 $m^2 \cdot g^{-1}$. CDC-TiC is also almost completely microporous with a dominating pore size of 0,7 nm [47]. Specific capacitances up to 152 $F \cdot g^{-1}$ in organic electrolytes have been reported for electrodes prepared from CDC-TiC [19, 48].

Silicon carbide (SiC) derived carbon is another common CDC, but it can have a lower surface area and a smaller average pore size compared to CDC-TiC, resulting in a lower ability to adsorb cations from organic electrolyte. Therefore, it is necessary to post-treat CDC-SiC with for example CO_2 or etch the carbon material by steam or water vapour to improve the pore-size distribution. [20] Specific capacitances up to 129 $F \cdot g^{-1}$ in organic electrolytes have been reported for electrodes produced from CDC-SiC [19, 48]. However, the cost of SiC can be 4 times lower than the cost of TiC (manufacturer's data) [49], resulting also in a desirable lower price of EDLC electrodes.

1.3.2 Carbon black

Carbon blacks are a group of materials that have near spherical carbon particles of colloidal size [8]. Their morphology is specified at different levels: particle, aggregate, and agglomerate. Carbon black (CB) particles covalently bond rapidly to form aggregates, the aggregates can be further bound together by van der Waals forces in more loosely associated agglomerates with a typical size of 10-100 µm. [50] Carbon blacks are produced by the partial combustion or thermal decomposition of hydrocarbons in the gas phase and their properties can be varied with feedstock and production process [8]. Carbon blacks are used as conductive additives in many batteries and supercapacitor electrodes, usually with a weight percentage of 5-10% [8, 51]. In this application, the dry powder conductivity of carbon blacks is approximately 10^{-1} to 10^{2} $S \cdot cm^{-1}$. By controlling the production process, the surface area of carbon black may be engineered up to 1500 $m^2 \cdot g^{-1}$ and

carbon blacks have also been used as the active material in supercapacitors. Specific capacitances in the order of 100 $F \cdot g^{-1}$ have been achieved with carbon black electrodes. [51]

CB's fine and highly branched structure makes them also ideally suited to filling inter-particle voids created between coarser particles. While carbon blacks improve the electrical contact between particles, the addition of carbon blacks also allows some manipulation of this inter-particle void volume. In carbon electrodes, the void volume can account for 25-40% of the total electrode volume and an excessive amount of voids can reduce the energy density of the device. Partially filling these voids with carbon black will also displace excess electrolyte which would otherwise increase the wet electrode weight and the cell cost. [8] Furthermore, carbon blacks may be cheaper than other carbonous materials and can be produced in large scale [51], further reducing the cell cost if some or all of the electrode's active material is substituted with carbon black.

1.4 Ionic liquids

As carbonous particles have a tendency for agglomeration, and agglomerates and inferior quality of dispersion of carbon particles in a matrix result in lower capacitance of EDLC electrodes [52], it is necessary to improve the dispersions, for example by using ionic liquids (ILs). ILs have been shown to efficiently disperse various carbon materials in different polymer mediums [32, 53].

Ionic liquids (ILs) are organic salts that are liquid at or near room temperature and have a melting point below 100^{o}C [54, 55]. Generally, they consist of an asymmetric organic cation and an inorganic anion [32, 56]. The most common anions and an imidazolium cation used in ionic liquids can be seen in Figure 1.5 and melting points of common ionic liquids in Table 1.2. ILs have low volatility and high electrochemical stability and they are chemically and thermally stable. At room temperature, low-viscosity ILs show electric conductivities at a level of 10 $mS \cdot cm^{-1}$. [55, 57]

Due to these properties, ionic liquids have attracted much attention for applications in many fields. One potential application for imidazolium-based room temperature ILs is dispersing carbon particles. It has been found that they can disperse carbon nanotubes (CNTs) by mechanical milling, forming a thermally stable gel. [57] In fact, studies show that imidazolium-ILs disperse CNTs more efficiently than common solvents, stabilizing them for a long time. Imidazolium-ILs have been used to disperse CNTs into polymer matrixes as well, for example into PS matrix or into SAN matrix. In

addition to CNTs, also graphite anode has been shown to electrochemically exfoliate into graphene sheets in an aqueous electrolyte containing $BMImBF_4$ or BMImCl ionic liquids. [32, 53]

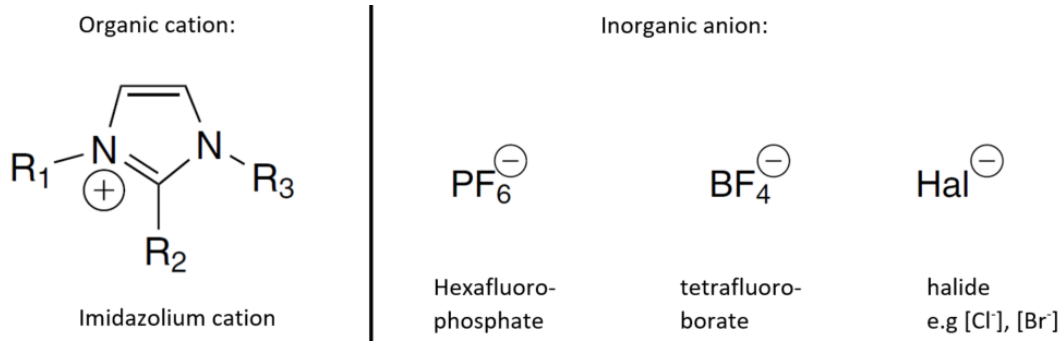

Figure 1.5. Common inorganic anions and imidazolium cation used in ionic liquids, where -R_n marks an alkyl chain [58]

For the use of ILs in supercapacitors, they should be electrochemically stable and conductive. The halide anions are the least electrochemically stable anions used in ionic liquids, while for example PF_6^- and BF_4^- are much more stable. [58] The ionic conductivity of the pure ionic liquid depends greatly on the cation size, longer alkyl chains result in noticeably smaller ionic conductivities [59]. An example of a good ionic liquid that combines good conductivity (12 $mS \cdot cm^{-1}$) with good electrochemical stability (4,3 V electrochemical window) is 1-ethyl-3-methylimidazolium tetrafluoroborate ($EMImBF_4$) [58].

Table 1.2. Melting points of common ionic liquids (manufacturer's data [60])

Ionic liquid	$EMImBF_4$	$EMImPF_6$	EMImCl	EMImBr	$BMImBF_4$	BMImCl
Melting point [^oC]	15	58	77	70	-71	70

Although ionic liquids are often referred to as green solvents due to their very low volatility compared to many organic solvents, they can still be potentially toxic when spilt into environment. In many studies a clear trend is seen that from all the tested cations, the imidazolium cation shows the highest toxicity in general and the longer the alkyl chains in the imidazolium cation are, the more toxic the ionic liquid is. In comparison to common organic solvents, e.g. dichloromethane and ethanol, ILs have been found to be 4-5 times more toxic. However, the role of anion in toxicity remains unclear and mostly it has been reported, that anions in ionic liquids do not affect the ecotoxicity, but are associated with determining the physical and chemical properties of ionic liquids. [61, 62]

1.5 Characterisation methods

Two characterisation methods used in this work, solution rheology and membrane's capacitance, are described in more depth in the following subchapters, for a deeper understanding of the results presented later.

1.5.1 Solution rheology

Rheology is used to describe the deformation and flow behaviour of matter, mostly fluids. A rheometer can be used to measure the shear stress τ and the shear rate $\dot{\gamma}$ of a liquid. The viscosity η is defined as $\eta \equiv \tau / \dot{\gamma}$. [63] The rheometers operate with continuous rotation or with rotational oscillation. In both cases the liquid sample is put between two plates, the lower of which is stationary, and the upper plate can be moved parallel to the lower plate, applying shear on the sample. [64]

In a continuous rotational test, the shear rate [s^{-1}] is increased stepwise to a maximum value and the resulting shear stress [Pa] is measured for each shear rate. The results of a rotational test can be presented as a flow curve graph that shows the resulting shear stress values or corresponding shear viscosity values [Pa·s] (Figure 1.6). If a fluid's internal flow resistance is independent of the shear rate, it is called a Newtonian liquid and its function of viscosity over the shear rate is a straight line. For liquids with shear-thinning flow behaviour, the viscosity decreases at higher shear rates and this behaviour is typical for polymer solutions, polymer melts and suspensions. For liquids with shear-thickening flow behaviour, the viscosity increases at higher shear rates. This behaviour is seen quite rarely and can be seen for example in samples with a high solid content such as ceramic suspensions. [65, 66]

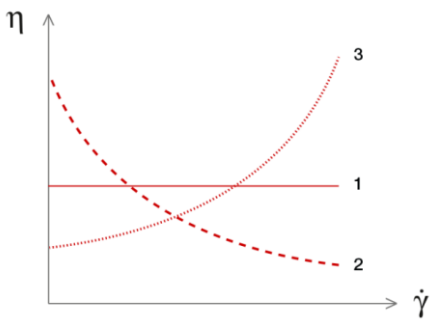

Figure 1.6. Flow curves of 1) Newtonian liquids, 2) shear-thinning liquids, 3) shear-thickening liquids in a plot of shear viscosity vs shear rate [65]

The abovementioned shear-thinning behaviour of polymer solutions is explainable with the entanglement of polymer chains. At rest, the long polymer chains are entangled with each other. Under shear the molecules are disentangled, and the resulting individual molecules have less flow resistance than entangled superstructures. This results in decreasing viscosity values at higher shear rates. Suspensions which have agglomerated primary particles have also shear-thinning behaviour: at rest, the agglomerates in the suspension enclose parts of the liquid and immobilize it, under shear these agglomerates increasingly disintegrate into smaller aggregates which show less flow resistance and free the formerly immobilized liquid for movement. [67]

The viscosity of a solid particle suspension in a polymer liquid depends on the volumetric concentration of the solid particles. As progressively more solids are added to the suspending liquid, the viscosity increases. In concentrated suspensions where more than 20 vol% are solid particles, even modest differences in particle size change how the particles slide past each other and change their maximum possible packing density. It has been shown that at a specified volumetric concentration, suspensions containing particles of at least two or three different sizes have a smaller viscosity when compared to a suspension containing particles of uniform size. [68]

Shear-thinning behaviour has been also noted for some ionic liquids. Burrell *et al.* studied five aprotic ionic liquids and of those, two were found to shear-thin (BMImCl and $EMImNTf_2$). They concluded that the ionic nature of the ionic liquid had little influence on the non-Newtonian flow but instead some other molecular interaction was implicated, specific to the functional groups of the cation. In the case of these two shear-thinning ionic liquids, the hydrogen at the C-2 position was not substituted with a functional group and this has been implicated to lead to strong intermolecular interactions at the C-2 position. These interactions are significantly reduced when the hydrogen is replaced by another functional group. In their study, when the C-2 hydrogen in $EMIm^+$ cation was replaced with a thiol group, the shear thinning did not occur. They suggested that the active proton at the C-2 position can form hydrogen bonds which can lead to the formation of aggregates. [69]

Suspensions can also have a rheologic behaviour more complex than those mentioned above. Various concentrated or semi-dilute suspensions have shown a unique three-regime flow curve: two shear-thinning regions at low and high shear rates, separated by a shear-thickening (or plateau) region over intermediate shear rates (Figure 1.7). The shear-thinning at low shear rates is mainly

attributed to the breaking up of large agglomerates into smaller particles, as mentioned above. Such structural transformation is controlled by dominant Brownian forces and the hydrodynamic forces have a minor contribution. Beyond a critical shear rate, a shear-thickening region appears where the lubricating hydrodynamic forces dominate and form the particles into highly anisometric and arranged “hydroclusters” (Figure 1.7), which are driven and sustained by the applied shear field. The nature of the shear-thickening depends on the parameters of suspended phase and the suspending medium (e.g. particle sizes and shapes, suspended phase volume). If the dispersion is composed of particle aggregates or fillers such as fumed silica or carbon black, the second regime of shear-thinning can be attributed to particle breakage due to extreme forces and thixotropy (time-dependent viscosity). [50, 70, 71]

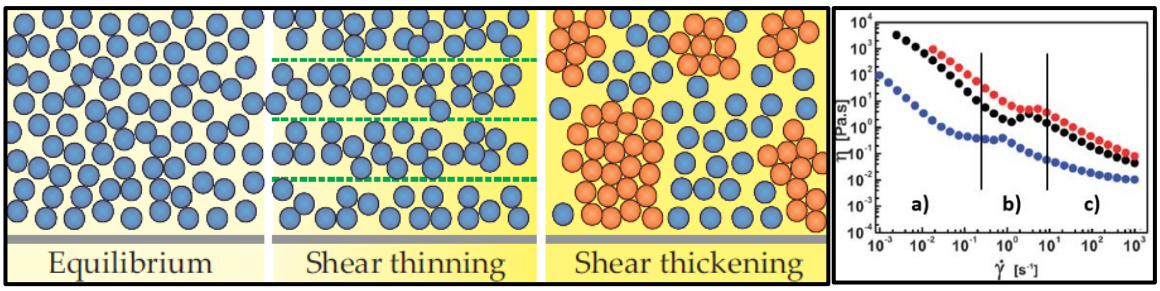

Figure 1.7. On the left: schematic of shear thinning (agglomerates are broken and particles become organised in flow) and shear thickening behaviour (formulation of hydroclusters) [71]. On the right: an example of three-regime flow curve, where a - is the shear-thinning region, b - shear-thickening region, and c - the second shear-thinning region [50]

1.5.2 Membrane’s capacitance

Capacitance is one of the key performance parameters evaluated when studying supercapacitor electrodes. Specific capacitance is the capacitance normalized by the weight of the active material and is calculated to compare the performance between electrodes with different masses. Evaluating the capacitance of materials can be done by using several different electrochemical techniques like cyclic voltammetry (CV), constant current method and electrochemical impedance spectroscopy, but CV is one of the most commonly used techniques. [13] All of these different analytical methods should yield the same capacitance for the same material in the same cell construction, if the measurement duration is equal [72].

Cyclic voltammetry applies a potential to the working electrode which linearly sweeps back and forth between two potentials. This potential range is limited by the electrolyte’s operating stability.

Scanning the potential range results in a time-dependent current and plotting this current (*I*) against the scanned potential (*E*) yields a cyclic voltammogram curve for capacitance analysis. Theoretically, a rectangular CV (Figure 1.8A) resembles an ideal capacitor. However, EDLC materials do not behave ideally and this results in a deformed rectangular shape (Figure 1.8B). From these curves, capacitance can be evaluated by dividing the integrated area under the CV curve with the potential scan rate and with the potential range. [13]

Potential scan rate has a significant effect on the measured capacitance. At lower rates, for example at 0,005 $mV \cdot s^{-1}$, the CV curves have a near ideal capacitive behaviour with a rectangular shaped curve. Increased scan rates distort the ideal CV curve and at extreme scan rates, the electrochemical kinetics cannot compete with the rapid change in potential. This will lead to a decline in performance as the micropores in active material will be underutilized. [13]

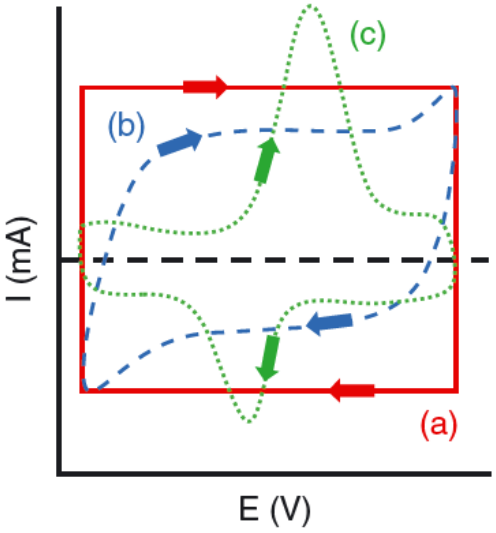

Figure 1.8. CV curves of a) the ideal capacitor, b) an EDLC material, and c) a pseudocapacitive material [13]

The electric double-layer capacitance intrinsically depends on the electrode potential, therefore the capacitance of the EDLC should be expressed as a function of cell voltage. The differential capacitance C_{dif}(V) is defined as the capacitance at a cell voltage (V) and can be obtained from the cyclic voltammetry by converting the CV current to the differential capacitance $C_{dif} = I \cdot a^{-1}$, where *I* is the CV current and *a* is the scan rate of the CV. [72]

The integral capacitance C_{int} is the average of the differential capacitance C_{dif}(V) in a voltage region ΔV (Eq 1.2) and it can be used as the representative capacitance of the electrode or the supercapacitor [72].

$$C_{int} = \frac{\int C_{dif}(V)dV}{\Delta V} \quad (1.2)$$

It should be also regarded that the capacitance of a three-electrode cell (C_{three}) is 2 times the capacitance of a two-electrode cell (C_{two}) when containing the same electrode (Eq 1.3) [72, 73].

$$\mathrm{C_{three}} = 2 \times \mathrm{C_{two}} \quad (1.3)$$

The specific capacitance of a three-electrode cell ($C_{g\text{-}three}$) is 4 times the specific capacitance of a two-electrode cell ($C_{g\text{-}two}$), if the weight of one electrode (m) is equal for the positive electrode and negative electrode in a two-electrode cell and for the electrode in a three-electrode cell, because

$$\mathrm{C_{g\text{-}three}} = \frac{\mathrm{C_{three}}}{m} \quad (1.4)$$

and

$$\mathrm{C_{g\text{-}two}} = \frac{\mathrm{C_{two}}}{2m} \ , \quad (1.5)$$

therefore, from the equations 1.3-1.5 it follows that

$$\mathrm{C_{g\text{-}three}} = \frac{\mathrm{C_{three}}}{m} = \frac{2 \times \mathrm{C_{two}}}{m} = \frac{2 \times \mathrm{C_{g\text{-}two}} \times 2m}{m} = 4 \times \mathrm{C_{g\text{-}two}} \ .[72, 73] \quad (1.6)$$

Thus, for the comparability sake of the obtained results in different studies, the specific capacitance is usually calculated as the capacitance per weight of active material contained in one electrode and the corrective multiplier 2 (from Eq 1.6) is used for two-electrode cells to compensate for the difference between two- and three-electrode configurations. Thus, the formula for specific integral capacitance $C_{int\text{-}specific}$ calculation for two-electrode cells obtains the shape:

$$\mathrm{C_{int\text{-}specific}} = \frac{2 \times \mathrm{C_{int}}}{m} = \frac{2 \times \int C_{dif}(V)dV}{m \times \Delta V} \ , \quad (1.7)$$

where C_{int} is the integral capacitance of the two-electrode cell and m is the weight of the active material in one electrode. [6, 40, 72-74]

2 EXPERIMENTAL PART

2.1 Materials

- N,N-dimethylformamide (DMF) – Sigma-Aldrich, ≥ 99.8%, Germany
- 1,2-Dichloroethane (DCE) – Emplura, ≥ 99.5%, France
- Poly(styrene-co-acrylonitrile) (SAN) – Polimeri Europa, average molar weight 180 000 g mol^{-1} by dynamic light scattering (DLS), Italy
- 1-ethyl-3-methylimidazolium tetrafluoroborate ($EMImBF_4$) – io-li-tec Ionic Liquids Technologies, 99%, Germany
- Carbon black (CB) – Timcal, Super C65, BET SSA 62 $m^2 g^{-1}$, Switzerland
- Silicon Carbide derived carbon (CDC-SiC) – Skeleton Technologies, steam post-treated, Estonia
- Titanium Carbide derived carbon (CDC-TiC) – Skeleton Technologies, Estonia

2.2 Instruments

- Retsch PM 100 (Germany) planetary ball mill was used to grind the CDC particles (Figure 2.1A).
- The weight of the solution components was measured with scale by Kern & Sohn (Germany).
- Node ultrasonic homogenizer Bandelin Sonoplus (Germany) was used with a MS 73 microtip probe (diameter 3 mm) to disperse the carbon particles in the solvent.
- Mettler Toledo Seven Compact (USA) conductivity meter was used to measure the electric conductivities of solutions and dispersions (Figure 2.1B).
- For solution rheology measurements an Anton Paar (Austria) rheometer, model Physica MCR 501 was used. (Figure 2.2A).
- The electrospinning setup consisted of a single syringe pump by New Era Pump Systems (USA), high voltage DC power supply by Gamma High Voltage Research (USA), and a self-constructed rotating cylinder collector (Figure 2.4).
- The morphology of electrospun membranes and carbonous additives was studied with scanning electron microscope (SEM) Gemini Zeiss Ultra 55 (Germany).

- The weight of the membrane samples was measured with scale Mettler Toledo AE163 (USA) for density calculations and specific capacitance calculations.
- Instron 5866 (USA) tensile testing machine with a 2,5 kN load cell was used to study the mechanical properties of electrospun membranes (Figure 2.1C). Bluehill 3 (USA) software was used to calculate the tensile stress values at maximum load for membranes.
- Conductivity meter High Resistance Low Conductance Meter HR 2 by AlphaLab (USA) was used to measure the conductance of membranes (Figure 2.2B).
- Thickness of the membranes was measured with Sony Magnescale U30 Digital Indicator (Japan) for membrane density and conductivity calculations (Figure 2.2C).
- Kelvin-1042 sorptometer by Costech International Instruments (Italy) was used for BET-analysis of CDCs and two membranes.

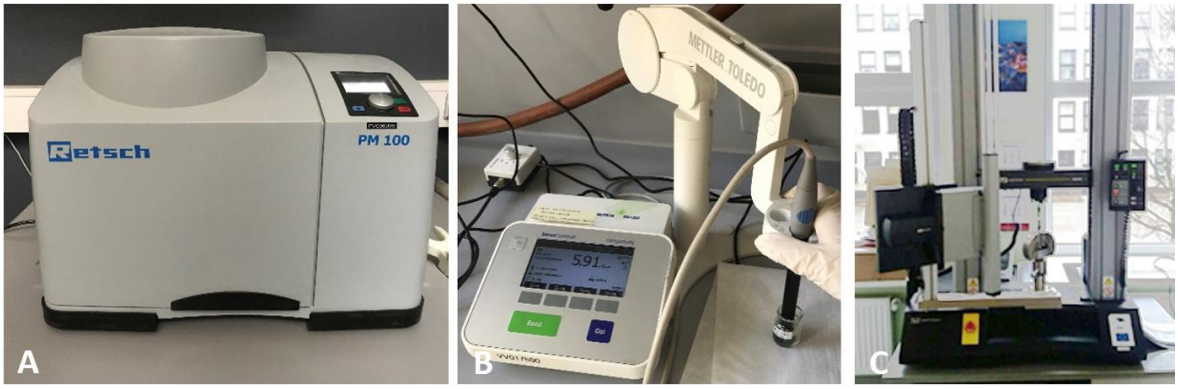

Figure 2.1. Used instruments: A – planetary ball mill, B – solution conductivity meter, C – tensile tester

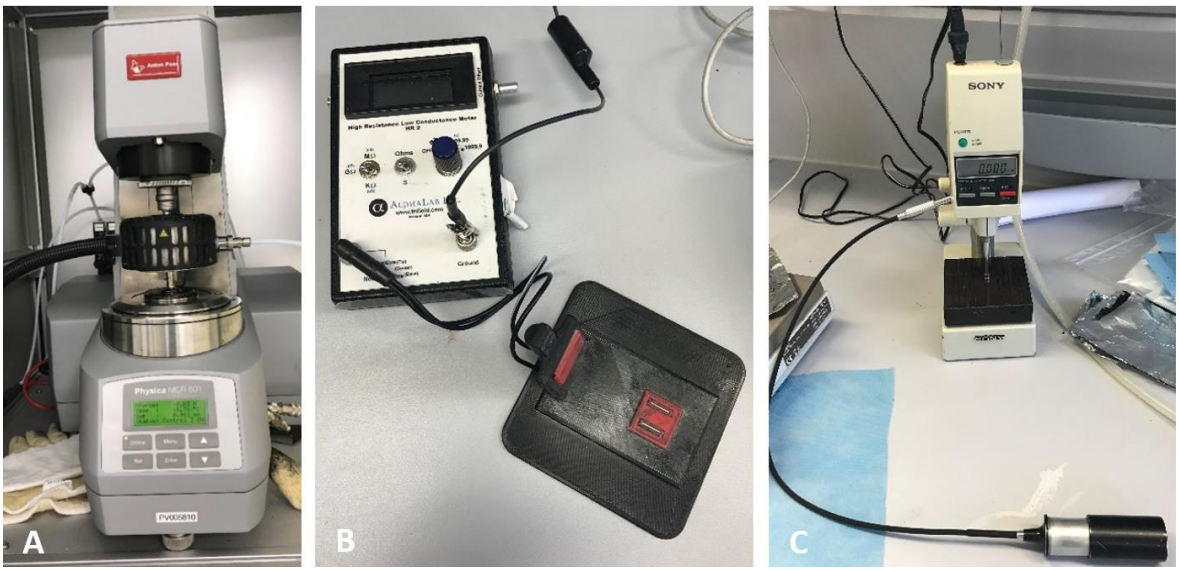

Figure 2.2. Used instruments: A – rheometer, B – conductivity meter, C – thickness measuring device

2.3 Grinding of carbide-derived carbons

The CDC-TiC and CDC-SiC were ground in a neutral N_2 atmosphere using a planetary ball mill to achieve a smaller particle size. Firstly, the CDC was weighed into a 0,5 L grinding jar in a glovebox and zirconium dioxide grinding balls with a 5 mm diameter were added to the jar. The jar was then closed, vacuumed and filled with nitrogen. The volume ratio of grinding balls to carbon was 4:1. The CDC was milled at a speed of 300 rpm for 1 hour. After milling, the grinding jar was cooled to the room temperature and CDC was transferred to a weighing bottle for storage.

2.4 Preparation of the electrospinning solutions and dispersions

Poly(styrene-co-acrylonitrile) was used as the polymer in the electrospinning solutions with a weight concentration of 15% in DMF and DCE solvents mixture. The 15 wt% concentration was chosen based on the literature review on electrospun SAN solutions (chapter 1.2.5), as in DMF solvent the 15 wt% was the critical entanglement concentration. DMSO solvent which has also been used for preparing the SAN electrospinning solutions was not suitable for this work, due to an insoluble precipitate formation when ionic liquid $EMImBF_4$ was added to the SAN in DMSO solution.

Weight concentration was used for preparing SAN solutions with 15 wt% concentration (Eq. 2.1). The weight ratio of carbonous additives to SAN was 1:1 and the weight ratio of ionic liquid to SAN was also 1:1. In all the solutions a mixture of DMF and DCE was used as the solvent, the weight ratio of DMF to DCE was 70:30. In some dispersions, a mixture of CDC and CB was used as the carbonous additive, in such case, the weight ratio of CDC to CB was 80:20. $EMImBF_4$ was used as the ionic liquid in this work and henceforth will be addressed as IL.

$$C\ (polymer) = \frac{m\ (polymer)}{m\ (polymer)+m\ (solvent)} \times 100\%\ , \tag{2.1}$$

where *C* is the concentration of polymer solution.

Two different solution preparation methods were used in present work, named as method 1 (M1) and method 2 (M2).

2.4.1 Method 1

With the method 1, firstly a dispersion of CDC in DMF was prepared in a weighing bottle by ultrasonicating the mixture for 2 hours in an ice bath. Then SAN was added to the dispersion, the weighing bottle was sealed with parafilm tape, the mixture was heated to 65^{o}C and stirred with a magnetic stirrer for 24 hours to dissolve the polymer. Thereafter, a solution of $EMImBF_4$ in DCE was prepared in a separate weighing bottle by mixing it with a magnetic stirrer for 30 minutes at room temperature. Then the IL-DCE solution was added to the SAN-CDC-DMF dispersion. The resulting mixture was further mixed for 24 hours at 65^{o}C to obtain a homogeneous dispersion. The schematic for dispersion preparation can be seen in Figure 2.3.

With method 1, only dispersions containing CDC could be prepared. When CDC and CB blend was used, it was not possible to ultrasonicate the mixture in only DMF as it was too thick. Altogether 6 electrospinning solutions and dispersions were prepared using method 1 and henceforth will be referred to by their solution names as shown in Table 2.1.

Table 2.1. Prepared electrospinning solutions and dispersions with method 1

Solution name (M1)	SAN	SAN+IL	SAN+IL+TiC	SAN+TiC	SAN+IL+SiC	SAN+SiC
Carbonous additives	–	–	CDC-TiC	CDC-TiC	CDC-SiC	CDC-SiC
Ionic liquid	–	$EMImBF_4$	$EMImBF_4$	–	$EMImBF_4$	–

2.4.2 Method 2

With the method 2, pure CDC or CDC+CB blend in ratio of 80:20 was used. A dispersion of carbonous additives in DMF and DCE solvents mixture was prepared in a weighing bottle by ultrasonicating carbon-solvent mixture for 2 hours in an ice bath. During the ultrasonication, some of DCE evaporated due to the higher volatility than that of DMF and therefore the weight of the mixture was checked every 30 minutes. If the weight had decreased, the missing amount of DCE was added to the mixture and the ultrasonication process was continued. After ultrasonication, SAN was added to the dispersion. The weighing bottle was then sealed with parafilm tape, heated to 65^{o}C, and stirred with a magnetic stirrer for 24 hours to dissolve the polymer. Then, $EMImBF_4$ was added to the dispersion and the mixture was further mixed for 24 hours at 65^{o}C. The addition of $EMImBF_4$ to the dispersion resulted immediately in a white precipitate formation which dissolved again completely within 25 minutes. This formation of precipitate was not seen with method 1. The schematic for dispersion preparation with method 2 can be seen in Figure 2.3.

Altogether 5 electrospinning solutions and dispersions were prepared using method 2 (Table 2.2). With method 1 it was observed that the membranes without IL (SAN, SAN+TiC, SAN+SiC) were not removable from the collector foil due to very low mechanical strength. Therefore, no dispersions without IL were prepared with method 2. Henceforth the solutions and dispersions prepared by method 2 will be referred to by their solution names as shown in Table 2.2.

Table 2.2. Prepared electrospinning solutions and dispersions with method 2

Solution name (M2)	SAN+IL	SAN+IL+TiC	TiC+CB	SAN+IL+SiC	SiC+CB
Carbonous additives	–	CDC-TiC	CDC-TiC + CB	CDC-SiC	CDC-SiC + CB
Ionic liquid	$EMImBF_4$	$EMImBF_4$	$EMImBF_4$	$EMImBF_4$	$EMImBF_4$

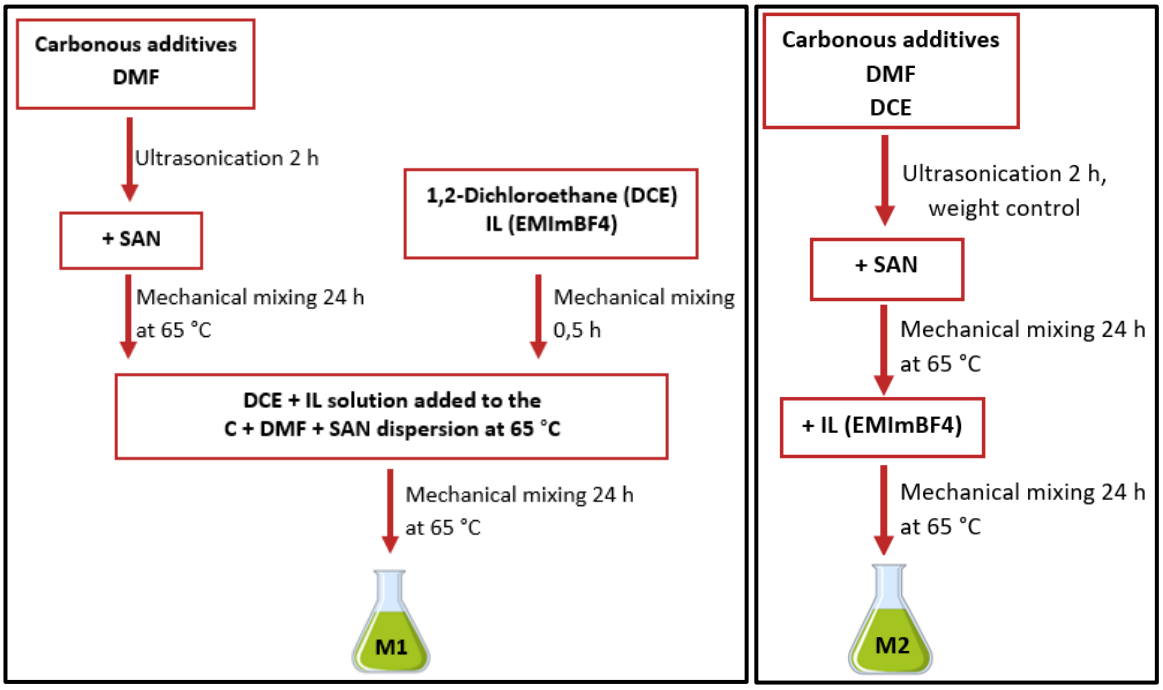

Figure 2.3. On the left – dispersion preparation schematic via method 1. On the right – dispersion preparation schematic via method 2

2.5 Characterisation of solutions and dispersions

2.5.1 Solution electric conductivity

The electric conductivity was measured for all the prepared solutions and dispersions to study and explain any correlations between the morphology of the electrospun membrane and the solution conductivity. The solution conductivity was measured using a conductivity meter and it was

measured 3 times for each solution from which the average electric conductivity was calculated. All the measurements were performed at room temperature between 20 – 23^{o}C.

2.5.2 Solution rheology

The flow curves (chapter 1.5.1) of all the solutions and dispersions were measured to study their shear viscosity. The rheology measurements were conducted with an Anton Paar rheometer using the cone and plate method in continuous rotation mode. The measuring cone CP25-2 with a diameter of 25 mm and 2^{o} angle was used for the measurements and the shear viscosity was measured at shear rates from 0,01 to 100 s^{-1}. The tests were conducted at room temperature, at 19 – 23^{o}C.

2.6 Electrospinning of solutions and dispersions

The prepared polymer solutions and dispersions were electrospun using a syringe pump and a rotating drum covered with aluminium foil as a grounded collector. The solution was held in a 1 ml syringe and a needle with an inner diameter of 0,1 mm was used. The solution pumping rate varied from 0,1 to 0,6 ml·h^{-1}. The electrospun membrane was collected onto the aluminium foil. The distance between the tip of the needle and the rotating collector was 10 – 13 cm and the voltage applied to the polymer solution was with most solutions between 15 and 18 kV. The electrospinning process was conducted at room temperature. The exact electrospinning parameters for all the solutions and dispersions can be seen in Table 2.3 and a photo of the used electrospinning setup in Figure 2.4.

Table 2.3. Electrospinning parameters of all the solutions and dispersions

Solution name (M1)	SAN	SAN+IL	SAN+IL+TiC	SAN+TiC	SAN+IL+SiC	SAN+SiC
Electrospinning parameters	10 cm 10 kV 0,4 ml·h^{-1}	10 cm 17 kV 0,1 ml·h^{-1}	10 cm 17 kV 0,2 ml·h^{-1}	10 cm 15 kV 0,6 ml·h^{-1}	12 cm 9 kV 0,15 ml·h^{-1}	10 cm 15 kV 0,6 ml·h^{-1}
Solution name (M2)		SAN+IL	SAN+IL+TiC	TiC+CB	SAN+IL+SiC	SiC+CB
Electrospinning parameters		10 cm 17 kV 0,6 ml·h^{-1}	10 cm 16 kV 0,4 ml·h^{-1}	13 cm 15 kV 0,2 ml·h^{-1}	10 cm 16 kV 0,4 ml·h^{-1}	13 cm 17 kV 0,2 ml·h^{-1}

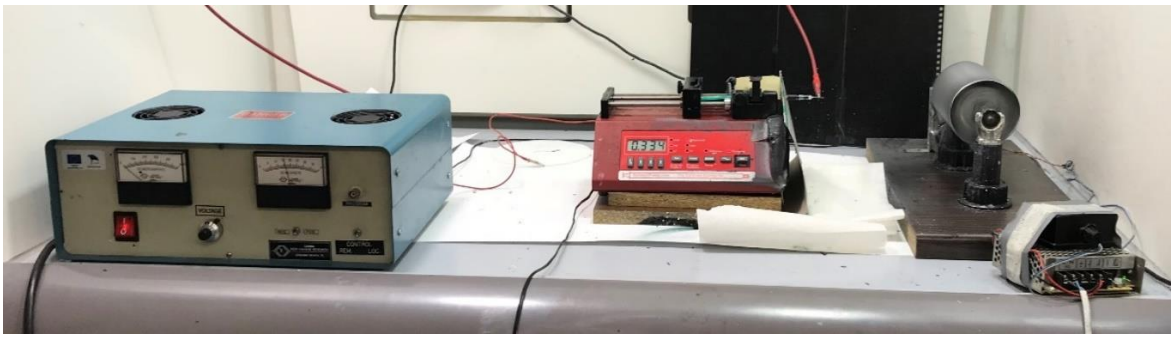

Figure 2.4. Electrospinning setup

2.7 Characterisation of membranes

2.7.1 Scanning electron microscopy

Scanning electron microscopy method was used to study the morphology of electrospun membranes. Fiber diameters were measured on the SEM images and the average fiber diameter was calculated. The prepared SEM samples were coated with gold before SEM imaging.

2.7.2 Density and areal density

To calculate the densities of electrospun membranes, 4 samples were cut from each membrane with an approximate size of 1,5 x 1,5 cm. These samples were weighed, their exact dimensions were measured, and their thickness was measured at 3 points.

For determining the average areal density of a membrane, the areal density values were calculated for the same 4 samples, by dividing the mass of the sample by the exact surface area of the sample (approximately 1,5 cm x 1,5 cm).

2.7.3 Tensile testing

Tensile testing method was used to study the effect of additives on the mechanical properties of electrospun membranes. For tensile testing, samples with a width of 1 mm and length of 4–5 cm were cut from the electrospun membranes. The sample thickness was measured with a digital thickness gauge. The tensile testing was conducted at ambient conditions. Gauge length was 1 cm and the strain rate 10 $mm \cdot min^{-1}$. As most of the fibers were aligned in one direction in the produced

nonwoven membranes due to the rotating collector, the tensile testing was conducted in the fiber direction.

The tensile testing was conducted for 10 samples from each membrane. The tensile stress at maximum load (Eq 2.2) and specific stress at maximum load (Eq 2.3) were calculated and reported for tested membranes. Henceforth, the tensile stress at maximum load will be simply addressed as tensile stress.

$$Tensile\ stress\ at\ maximum\ load = \frac{maximum\ load\ [\mathrm{N}]}{membrane\ thickness\ [\mathrm{m}] \times membrane\ width\ [\mathrm{m}]} \quad (2.2)$$

$$Specific\ stress\ at\ maximum\ load = \frac{maximum\ load\ [\mathrm{N}]}{membrane\ width\ [\mathrm{m}]} \times \frac{1}{average\ areal\ density\ [\frac{\mathrm{g}}{\mathrm{m}\times\mathrm{m}}]} \quad (2.3)$$

2.7.4 Electric conductivity

The electric conductance *G* of the membranes was measured to study the influence of conductive additives. The electric conductance was measured using a two-point method with a conductivity meter. The length of the electrodes was 1 cm and the distance between the two electrodes was also 1 cm. A sample of the membrane was laid on the electrodes so that the direction of the fibers was matching that of the electric current (Figure 2.5). After measuring the conductance, the thickness of the membrane was measured at 5 points and the electric conductivity σ of the membrane was calculated (Eq. 2.4).

$$\sigma = G \times \frac{l}{A} \quad , \quad (2.4)$$

where σ [µS·cm^{-1}] is the conductivity of the membrane, *G* [µS] is the measured conductance, *l* [cm] is the distance between the electrodes and *A* [cm^2] is the area of the cross-section of the electric current transmission (length of the electrode x thickness of the membrane).

The electric conductivity of the membranes depends also on the pressure which is applied to the membrane during measurement. Increased applied pressure results in a higher conductivity value, because forcing the fibers and particles into a more intense packing arrangement creates new contacts with neighbouring fibers and particles [75]. Therefore, for the comparison sake of prepared membranes, all the conductance measurements were performed with an 88,77 g load applied to the membranes (Figure 2.5).

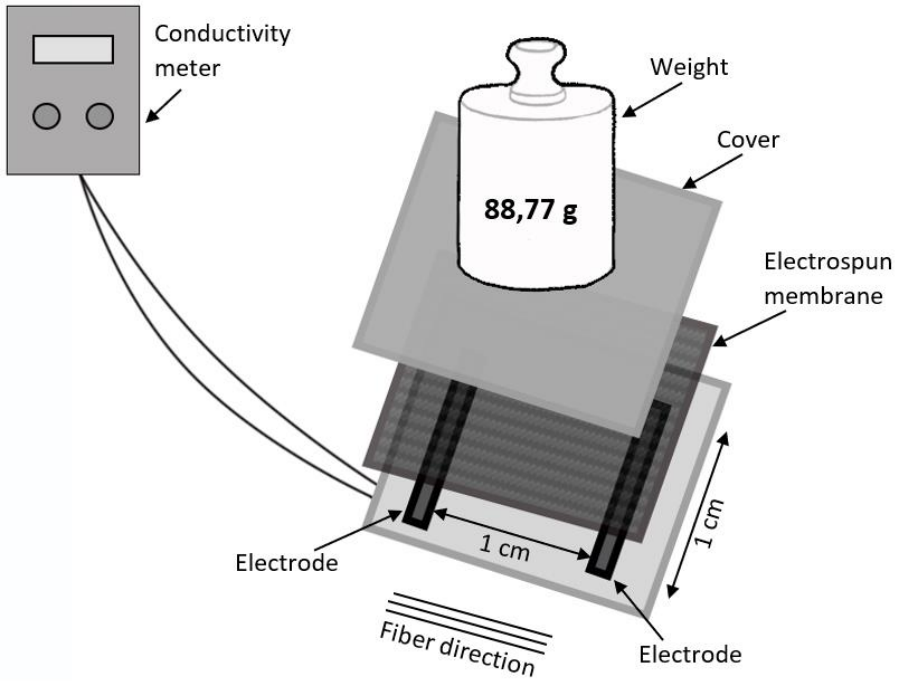

Figure 2.5. Schematic of the membrane conductance measurement

2.7.5 BET analysis

Before conducting the BET analysis, the ionic liquid was washed out from the membranes by immersing the membranes in ethanol for 3 x 24 hours. Subsequently, the membranes were dried in a neutral atmosphere at 105^{o}C. The specific surface area, total pore volume and micropore volume were measured for as-received and grinded CDCs, and for two electrospun membranes by low temperature N_2 adsorption method with a sorptometer. The degassing temperature for pure CDCs and membranes was 300^{o}C and 35^{o}C, respectively. Helium was used as the carrier gas during degassing.

2.7.6 Electrochemical characterisation

The electrochemical characteristics of electrospun membranes containing carbonous additives were studied by cyclic voltammetry (CV) method (chapter 1.5.3). The differential and integral specific capacitances of the active material in the membranes were calculated and specific capacitance vs voltage plots were analysed. An organic electrolyte triethylmethylammonium tetrafluoroborate in acetonitrile (TEMA/AN) was used for the electrochemical cell preparation.

Before preparing the cells for electrochemical testing, the electrospun membranes were annealed at 105^{o}C for 72 h to dry them by evaporating any water in the membranes. Then the annealed membrane was laid between aluminium foils, heated between a hot press to 75^{o}C and pressed for 1 minute at a pressure of 2,5 MPa (Figure 2.6A). The positive and negative electrodes were cut out from the pressed membrane using a cutting stencil (Figures 2.6B–2.6C), after which the thickness and weight of the electrodes were determined. A separator was laid on top of the heavier electrode (Figure 2.6D) and the lighter electrode was laid on top of the separator so that the electrodes were aligned exactly on top of each other. The electrode-separator-electrode assembly was put into the metal cell part (Figure 2.6E) and a metal weight plate was laid on top of the assembly to avoid any movement of electrodes (Figure 2.6F). An insulating Teflon strip was put along the inner wall of the metal cell to avoid its contact with the electrodes. The upper part of the metal cell was assembled on top of the bottom part and fastened with screws (Figure 2.6G), after which it was annealed at 105^{o}C for 72 h. After annealing, a filling device was attached to the cell (Figure 2.6H) and the cell was vacuumed for 10 minutes. After vacuuming, organic TEMA/AN electrolyte was injected through the filling device to the cell. The filling device was removed, the remaining hole was covered with a screw, and the electrolyte was let to immerse into the electrodes for 24 h. Finally, the electrochemical cyclic voltammetry tests were conducted on the assembled cells by Skeleton Technologies Ltd.

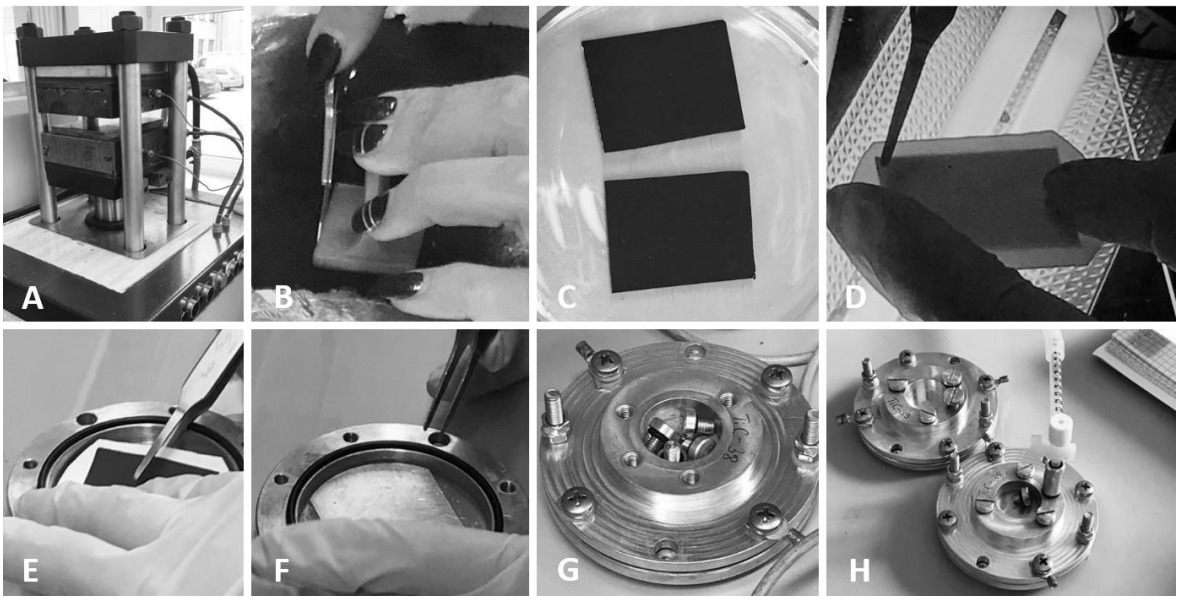

Figure 2.6. Electrochemical test cell preparation process. A – hot pressing, B – cutting out electrodes from the membrane, C – electrodes, D – separator on top of the electrode, E – laying the electrode-separator-electrode assembly in the metal cell, F – metal weight plate on top of the electrodes, G – assembled cell before annealing, H – vacuuming the cell after annealing

From the obtained cyclic voltammetry test results the differential specific capacitance values in $F \cdot g^{-1}$ corresponding to voltage values in V were calculated (Eq 2.5).

$$C_{\text{dif-specific}}(V) = \frac{2 \times I}{a \times m} \quad , \tag{2.5}$$

where *I* is the CV current, *a* is the scan rate of the CV, and *m* is the weight of carbon in one electrode.

The integral specific capacitance was calculated from $C_{dif\text{-}specific}(V)$ values by using numerical trapezoidal integration method. If the function is represented as a curve on a graph, then the integral is defined as the net area under that curve. Therefore, the area under the curve must be calculated by some indirect way, a popular one of which is the trapezoidal rule. The trapezoidal rule approximates the region under the graph of a function as trapezoids (Figure 2.7) and allows to calculate their individual areas according to equation 2.6. [76]

$$\int_{V_1}^{V_2} C_{\text{dif-specific}}(V)\, dV \approx (V_2 - V_1) \times \frac{C_{\text{dif-specific}}(V_1) + C_{\text{dif-specific}}(V_2)}{2} \tag{2.6}$$

If n points from the curve are known, the equation 2.6 can be applied n-1 times and then these n-1 areas of tiny trapezoids can be summed to calculate the whole area under the curve. The area under the curve can be divided by the voltage region ΔV to obtain the integral specific capacitance of the supercapacitor per weight of carbon in one electrode. In this work, all the CV curves were composed of approximately 3000 data points, making this trapezoidal numerical integration method sufficiently exact for evaluating the specific capacitances of produced supercapacitor electrodes. [76]

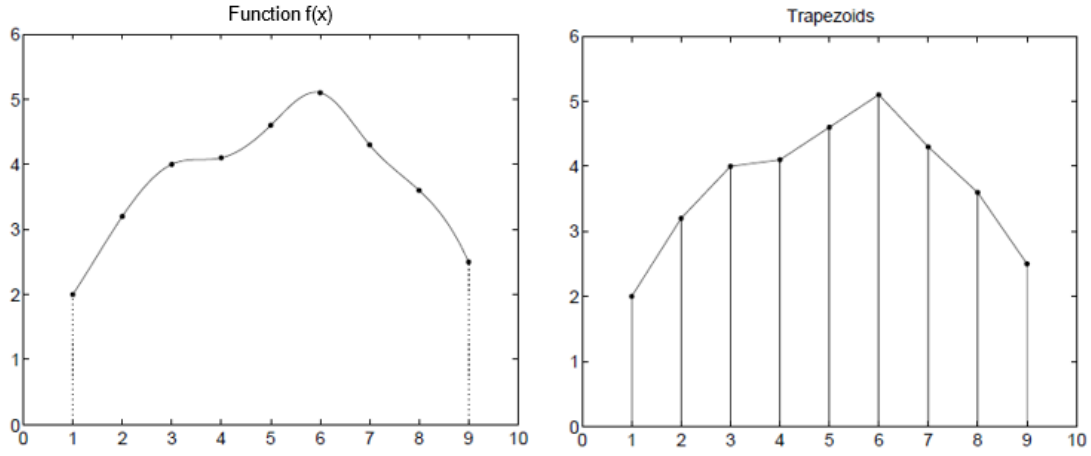

Figure 2.7. On the left: a curve of a function f(x), on the right: the trapezoidal approximation of the same curve [77]

3 Results and discussion

3.1 Effect of grinding on the morphology and porosity of CDC

The CDCs provided by Skeleton Technologies contain mixtures of several fractions with typical particle sizes between 0,5 and 10 µm. As the electrospun SAN fibers are significantly thinner, with a diameter of approximately 200 nm, the size of CDC particles should be reduced for their effective incorporation into SAN fibers through electrospinning. The impact of grinding on the porosity and specific surface area of CDCs was studied by BET analysis to ensure that most of the SSA was retained during grinding.

Morphology. The 1-hour grinding of CDCs with a planetary ball mill reduced the average particle size of both CDC-TiC and CDC-SiC, but the average size and the size distribution was larger for CDC-TiC after grinding, than for CDC-SiC (Figure 3.1). It can be further seen from the SEM images, that the largest particle size for ground CDC-TiC is approximately 20 µm, whereas for ground CDC-SiC the largest particles are 6 µm. The higher size reduction effect in the case of CDC-SiC might be due to its lower hardness when compared to CDC-TiC. The particle size distribution analysis, measured by DLS technique, shows that the average particle size for CDC-TiC after 1-hour grinding is approximately 800 nm (Figure 3.2).

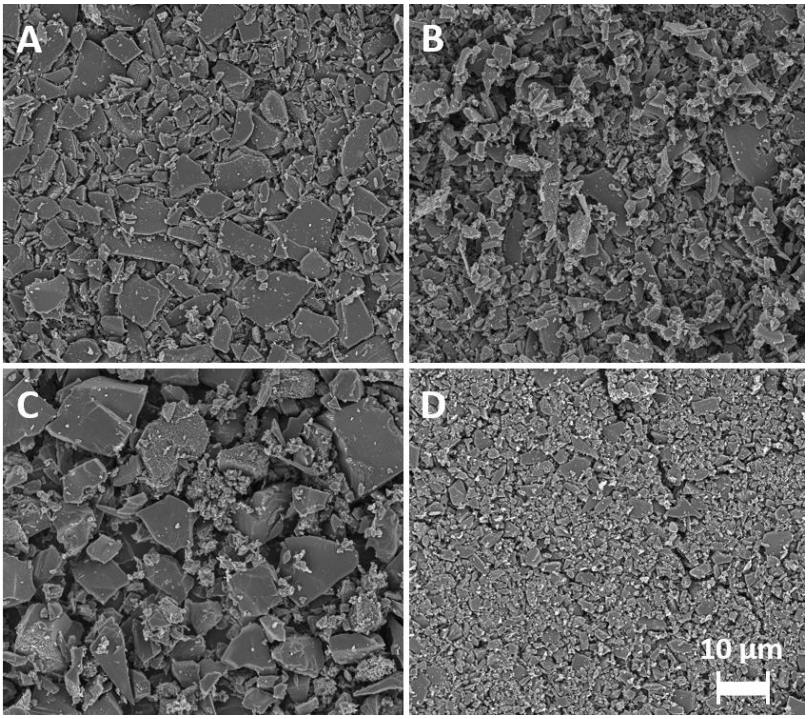

Figure 3.1. SEM images of CDCs. A – as-received CDC-TiC, B – 1 h ground CDC-TiC, C – as-received CDC-SiC, D – 1 h ground CDC-SiC. The scale bar corresponds to 10 µm on all the images

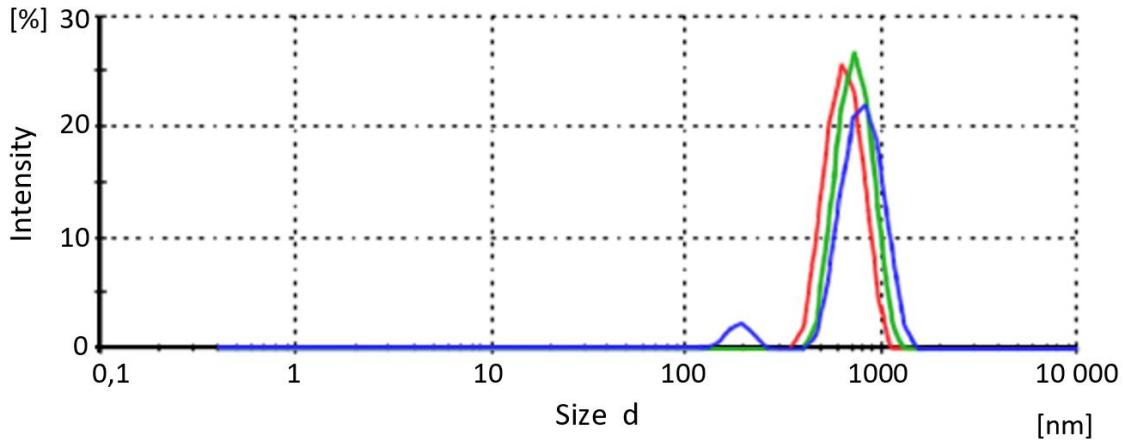

Figure 3.2. Particle size distribution by intensity for 3 samples of 1 h ground CDC-TiC

Porosity and SSA. The 1-hour grinding decreased the total porosity of both CDCs and as a result also their specific surface area by a small extent (Table 3.1). In the case of CDC-TiC, the decrease in SSA was only 3,5% while with CDC-SiC the SSA decreased by 15%, indicating that more pores collapsed during grinding and that the particle breakage was less brittle [78] in the case of CDC-SiC.

Table 3.1. The specific surface area and pore volume *V* [cm^3] per weight [g] of CDC (as-received and after grinding)

CDC	BET SSA [$m^2 \cdot g^{-1}$]	*V* (micropores) [$cm^3 \cdot g^{-1}$]	*V* (total porosity) [$cm^3 \cdot g^{-1}$]
As-received CDC-TiC	1633	0,57	0,77
1 h ground CDC-TiC	1576	0,51	0,74
As-received CDC-SiC	1542	0,38	0,81
1 h ground CDC-SiC	1306	0,40	0,71

3.2 Properties of electrospinning solutions and dispersions

3.2.1 Electric conductivity

The electric conductivity of the solution has a strong influence on the electrospinning process and on the resulting morphology of the electrospun membrane. Thus, the electric conductivities of all the solutions and dispersions were measured and the influence of IL, carbonous additives and different solution preparation methods on the conductivity of the dispersions was studied.

The electric conductivities of method 1 dispersions prepared without ionic liquid (SAN, SAN+TiC and SAN+SiC) were all approximately 2 $\mu S \cdot cm^{-1}$, measured at temperatures between 22,7 and 23,2^{o}C. The addition of ionic liquid to the dispersions increases their electric conductivity by three orders of magnitude. When comparing two dispersion preparation methods, the method 2 dispersions have higher electric conductivities than the method 1 dispersions (Figure 3.3). This can be due to the better dispersions obtained with method 2, when compared to method 1. During the ultrasonication of carbon particles and solvent mixture, there is 30 wt% more solvent present per the same amount of carbon in the case of method 2, allowing to disperse the carbon particles more homogeneously. The tendency that better dispersions result in higher electric conductivity, has also been observed and simulated in literature. It was explained with the shorter distances between neighbouring particles, which have then more opportunities to form a conductive network, leading to higher conductive probability [79].

When comparing the SAN+IL method 2 solution to dispersions containing IL and carbonous additives (e.g. SAN+IL+TiC M2), then a decrease in the conductivity can be observed, from 11 $mS \cdot cm^{-1}$ to around 8–9 $mS \cdot cm^{-1}$ (Figure 3.3). This indicates that the carbonous additives absorb some of the ionic liquid and solvent, reducing the amount of freely moving ions and thus the conductivity of the solution. Exchanging a part of the CDC with the conductive carbon black (CB) additive, resulted in a minor increase in the conductivity of the dispersions when compared to pure CDC dispersions. The conductivity of the CDC-TiC containing dispersions is a bit lower than that of the CDC-SiC containing dispersions. This can indicate that during the synthesis of the CDC-SiC, perhaps more conductive carbon allotropes were formed (e.g. graphite crystals or nanotubes) than in the case of CDC-TiC, leading to the higher conductivity of the solution, or the difference could be due to the different particle size of CDC-TiC and CDC-SiC and their different interactions with other dispersion components [19].

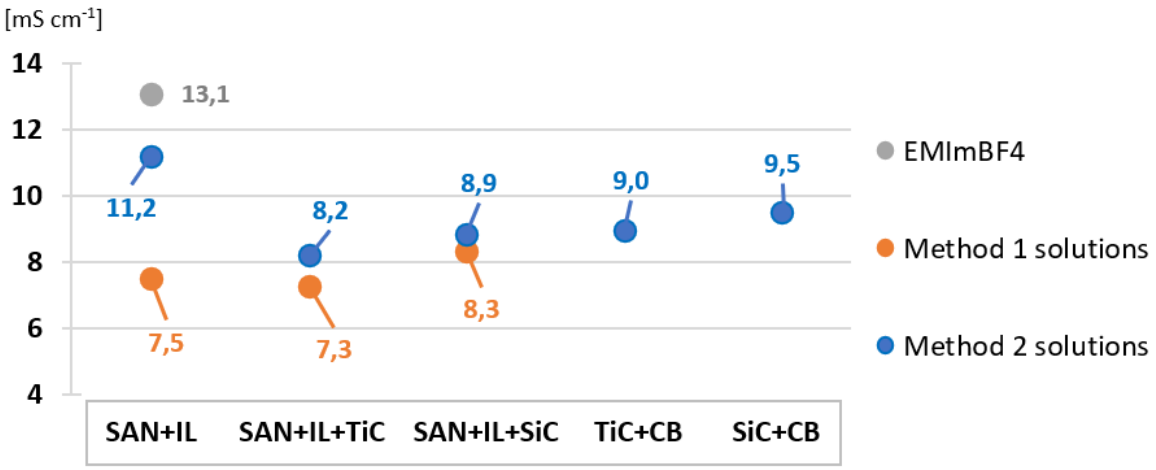

Figure 3.3. Electric conductivities of dispersions containing $EMImBF_4$ ionic liquid and electric conductivity of the pure ionic liquid in $mS \cdot cm^{-1}$

3.2.2 Rheology

The electrospinnability of a solution and the resulting morphology depends strongly on the viscosity of the solution, therefore the viscosity values at different shear rates were measured for all the solutions and dispersions. Additionally, the rheology measurements provided useful insight about how well the carbonous additives were dispersed and therefore allowed to compare different dispersions preparation methods.

The used ionic liquid $EMImBF_4$ showed interestingly a shear-thinning behaviour, indicating the existence of aggregates (Figure 3.4), which is not common for ionic liquids. Yet the same behaviour has been observed for some imidazolium-ILs, where similarly the hydrogen at the C-2 position of the cation is not substituted with a functional group. The latter can result in strong intermolecular interactions, leading to the formation of aggregates. [69] Both SAN + IL solutions have also shear-thinning behaviour (Figure 3.4), which is typical for polymer solutions. Throughout the shear rates, SAN + IL method 1 solution has considerably smaller viscosity values than SAN + IL method 2 solution. This can suggest that the solution prepared with method 1 was more homogeneous and the disentanglement of the long polymer chains was easier, resulting in reduced flow resistance compared to SAN + IL method 2 solution.

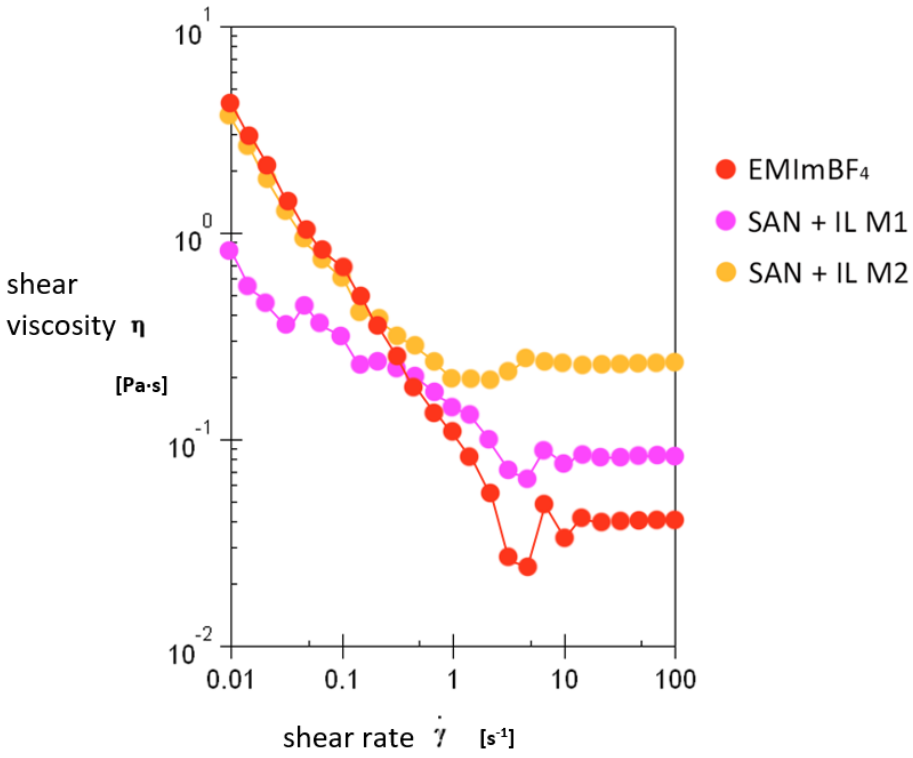

Figure 3.4. Flow curves of pure ionic liquid, SAN + IL solution prepared with method 1, and SAN + IL solution prepared with method 2

When CDC-SiC was added to these IL-containing solutions, the viscosity values of both, method 1 and method 2 dispersions, increased, and at low shear rates their shear viscosities were practically equal (Figure 3.5) as opposed to the solutions without CDC. However, at higher shear rates, the viscosity of SAN+IL+SiC method 2 dispersion decreased to a notably smaller level than the viscosity of the method 1 dispersion. From this rheological behaviour it can be deduced that during the shear, ionic liquid was able to help lubricate and disintegrate the CDC-SiC agglomerates into smaller aggregates in method 2 dispersion better than in method 1 dispersion, owing to different dispersion preparation methods. At lower shear rates, the viscosity of SAN + SiC dispersion without IL was smaller than that of the dispersions containing IL, however, at higher shear rates the opposite rheological behaviour could be observed (Figure 3.5). This further confirms that the ionic liquid aids in breaking up the carbonous agglomerates and reduces the flow resistance of the dispersion at higher shear rates.

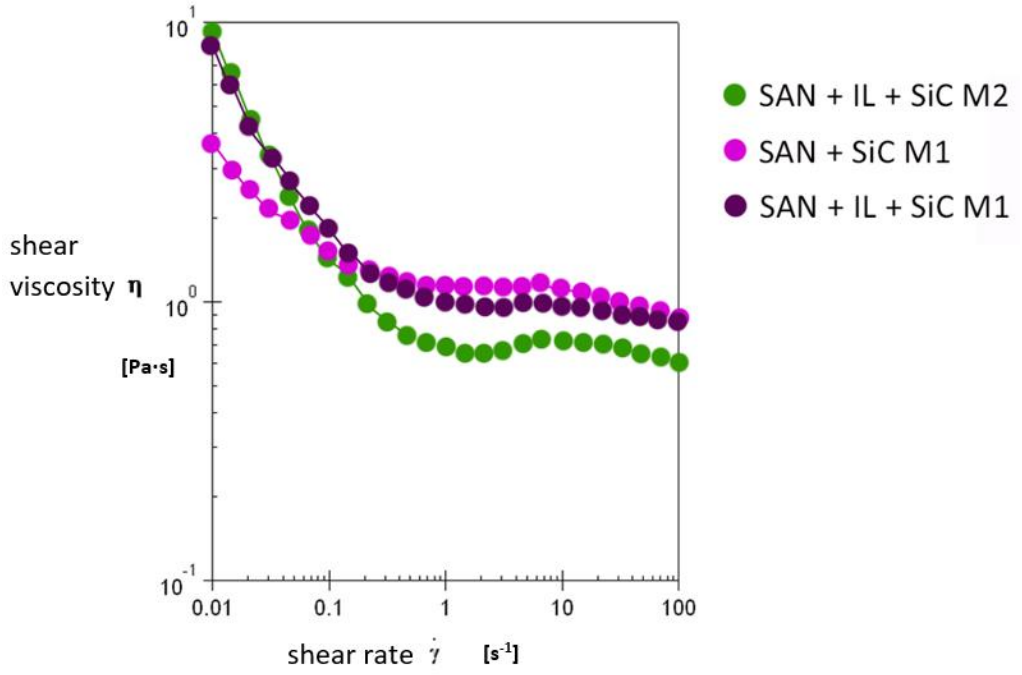

Figure 3.5. Flow curves of dispersions prepared with CDC-SiC: SAN + SiC dispersion without IL, prepared with method 1; and SAN + IL + SiC dispersions prepared with methods 1 and 2

The rheological behaviour of SAN+IL+SiC and SAN+IL+TiC dispersions prepared with method 2 are very similar, although the viscosity of SAN+IL+TiC is a bit lower throughout the shear rates than in the case of SAN+IL+SiC (Figure 3.6). This can be due to the larger size of CDC-TiC particles as seen from the SEM images. A higher amount of different sized particles can lead to the reduction in viscosity if the volume fraction of solids is more than 20% in the dispersion [68], which is the case in the prepared dispersions.

The dispersions containing CDC+CB blends show a distinct rheological behaviour, especially in the case of SiC+CB, where the three-regime flow curve can be seen (Figure 3.6): a shear-thickening region between two shear-thinning regions. This behaviour is associated with the formation of hydroclusters at intermediate shear rates (0,1 – 1 s^{-1} in this case) (chapter 1.5.1). This interesting three- (or two-) regime flow curve can be also vaguely observed for other prepared dispersions, however not as sharply as in the case of SiC+CB dispersion.

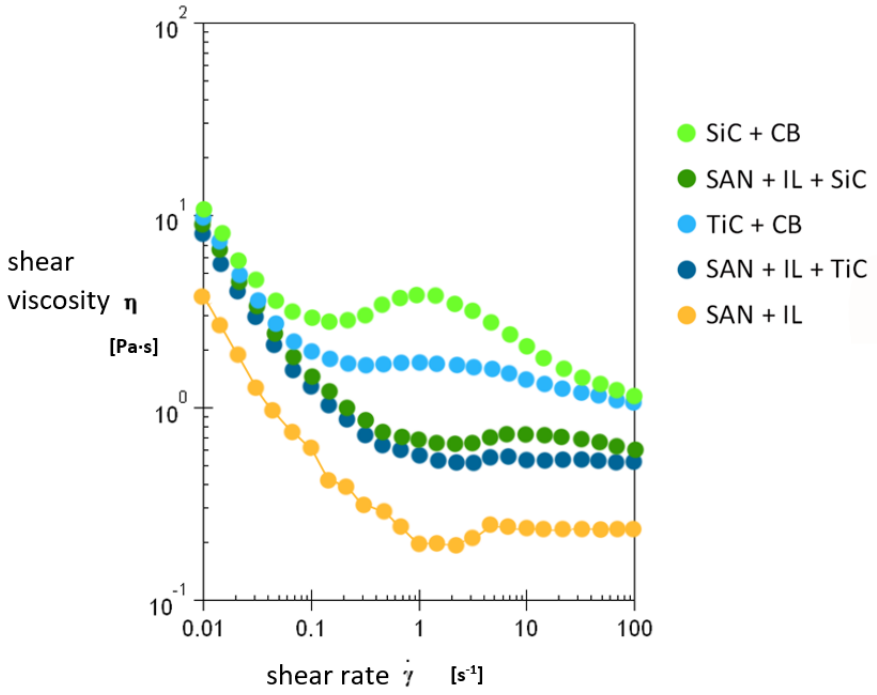

Figure 3.6. Flow curves of all the dispersions prepared with method 2

3.3 Properties of electrospun membranes

3.3.1 Morphology

The study on the morphology of electrospun membranes revealed, that the fiber diameter and the presence of defects like solvent beads strongly depended on the solution conductivity and viscosity. Firstly, the morphology of pure SAN membrane and the effect of IL on the fiber morphology is discussed. Secondly, the morphology of different carbonous additive containing membranes is studied.

The electrospun SAN membrane without any additives consists of very thin fibers (average diameter 158 nm) and spherical solvent beads (average diameter 2,5 µm) (Figure 3.7). When ionic liquid was added to the solution, the fiber diameter increased 1,5 times with method 1, and more than 3 times with method 2 (Figure 3.8). The method 2 solution had the highest electric conductivity of these solutions. In many studies the higher electric conductivity of the solution has been shown to lead to thinner fibers and therefore to an exact opposite behaviour [31, 33]. However, its effect on fiber diameter also depends on the interactions between the conductive additive and polymer solution, and in a few cases similarly an increase in the fiber diameter has

been observed when conductivity was improved by using conductive additives [80, 81], unfortunately no explanations were offered in these studies for the phenomenon.

In another study, it was found that when an ionic liquid was added to the polymer solution, then at lower IL concentrations (2,5 mol/L) the fiber diameter decreased, however, when the concentration was further increased (up to 10 mol/L), the fibers were thicker than the fibers at 0% IL concentration. It was explained that "the increase in the electrostatic force due to the increase in the conductivity delayed the onset of the bending instability and therefore shortened the fiber stretching process, resulting in larger fibers". [34] The same explanation may be applied to the results in this work, as the increase in solution conductivity is very abrupt when IL is added, from 2 $\mu S \cdot cm^{-1}$ to 11 $mS \cdot cm^{-1}$.

In addition to the conductivity, also higher solution viscosity influences the fiber diameter in the growing direction. As the viscosity values of SAN+IL M2 solution are higher compared to SAN+IL M1 solution (Figure 3.4), this can further justify the thicker fibers of the former, but also its smoother fiber surface and bead-free fibers when compared to the beaded SAN+IL M1 fibers (Figure 3.7).

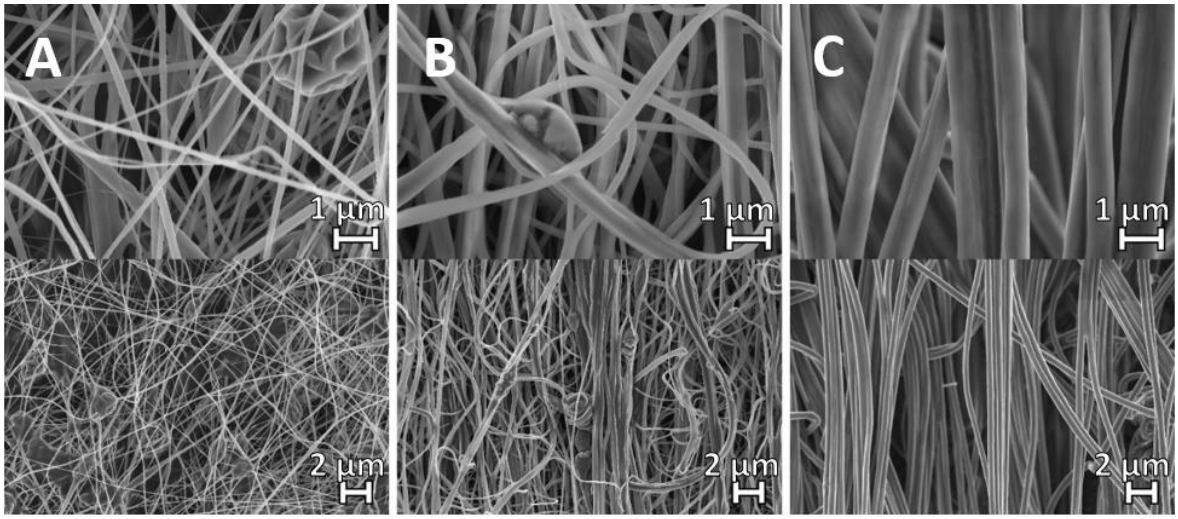

Figure 3.7. SEM images of A – SAN membrane, B – SAN+IL method 1 membrane, and C – SAN+IL method 2 membrane with different magnifications

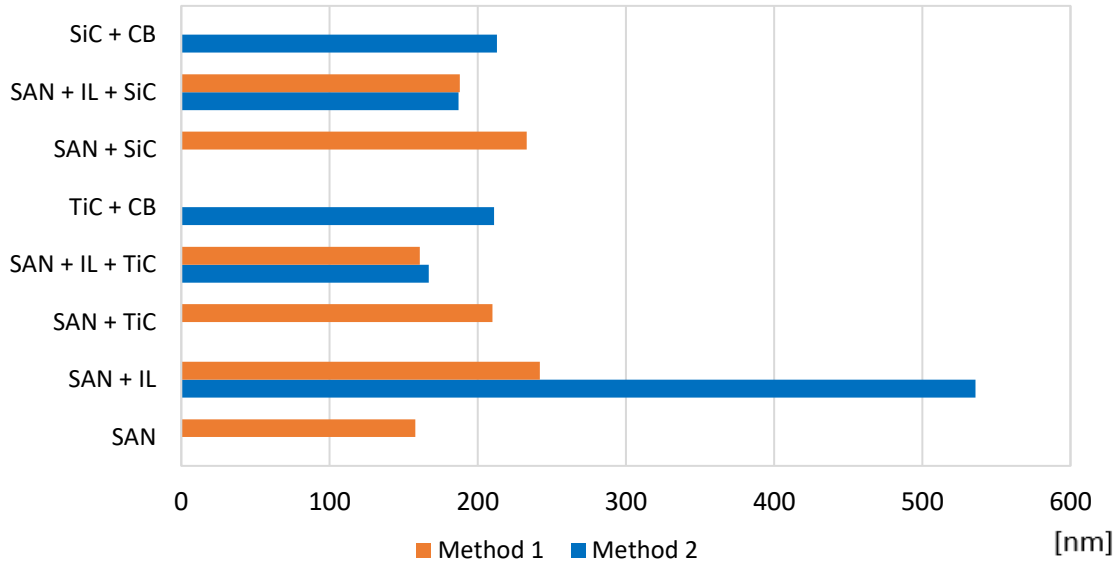

Figure 3.8. Average fiber diameters of all the electrospun membranes in nm

Although in the case of SAN+IL membranes there was a surge in fiber diameter, then with carbon-containing membranes the fiber diameter fluctuated only a little (Figure 3.8). Still, some conclusions can be drawn. Firstly, the membranes containing CDC but no ionic liquid (e.g. SAN + TiC) had thicker fibers when compared to membranes also containing ionic liquid (e.g. SAN + IL + TiC). The smaller fiber diameters of latter is explainable with their lower viscosity values at higher shear rates (depending on the pumping rate, the apparent shear rate at the needle opening was on the order of 10 – 100 s^{-1} with the used pumping rates and needle diameter). Furthermore, the CDC agglomerates were better dispersed in the membrane and their size was smaller when also ionic liquid was added to the dispersion, especially in the case of CDC-SiC (Figure 3.9).

From the SEM images it can be seen that the CDC particles are situated inside the fibers (Figure 3.10). The surface of the CDC-containing fibers is also notably rougher when compared to the fibers without CDC. Further, in places where larger CDC particles are coated with the polymer, pores can be seen in the polymer fiber surface (Figure 3.10). The porosity of electrospun SAN fibers is their most important advantage, as the open pores on the fiber surface allow the electrolyte ions to access the surface of the CDC particles, making it possible to use these membranes potentially as supercapacitor electrodes.

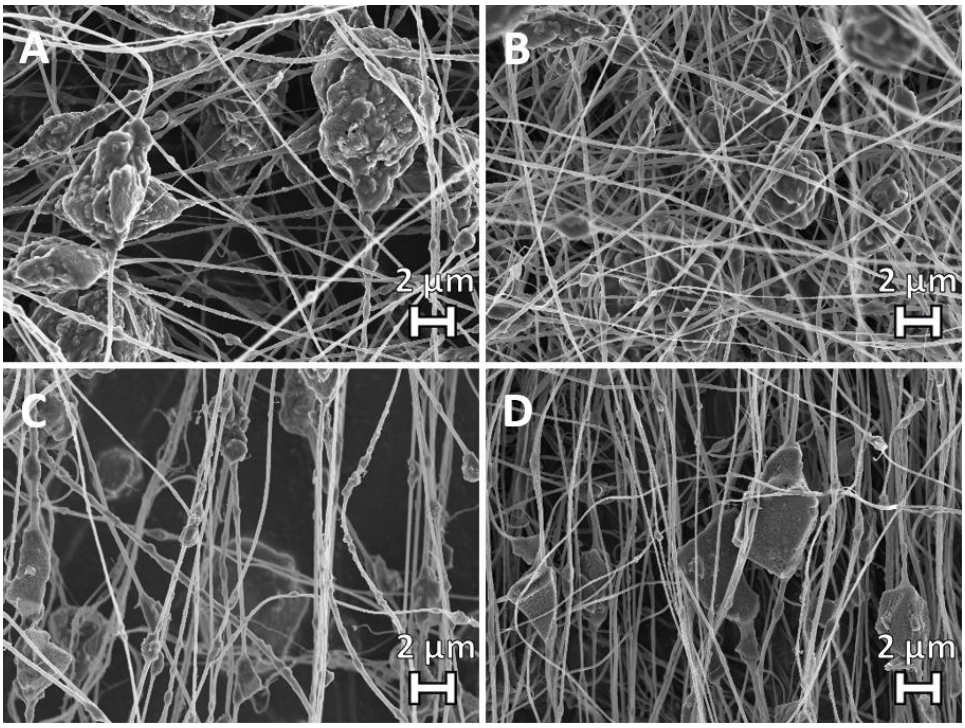

Figure 3.9. SEM images of membranes prepared with method 1: A – SAN+SiC, B – SAN+IL+SiC, C – SAN+TiC, D – SAN+IL+TiC, the scale bar on all the images corresponds to 2 µm

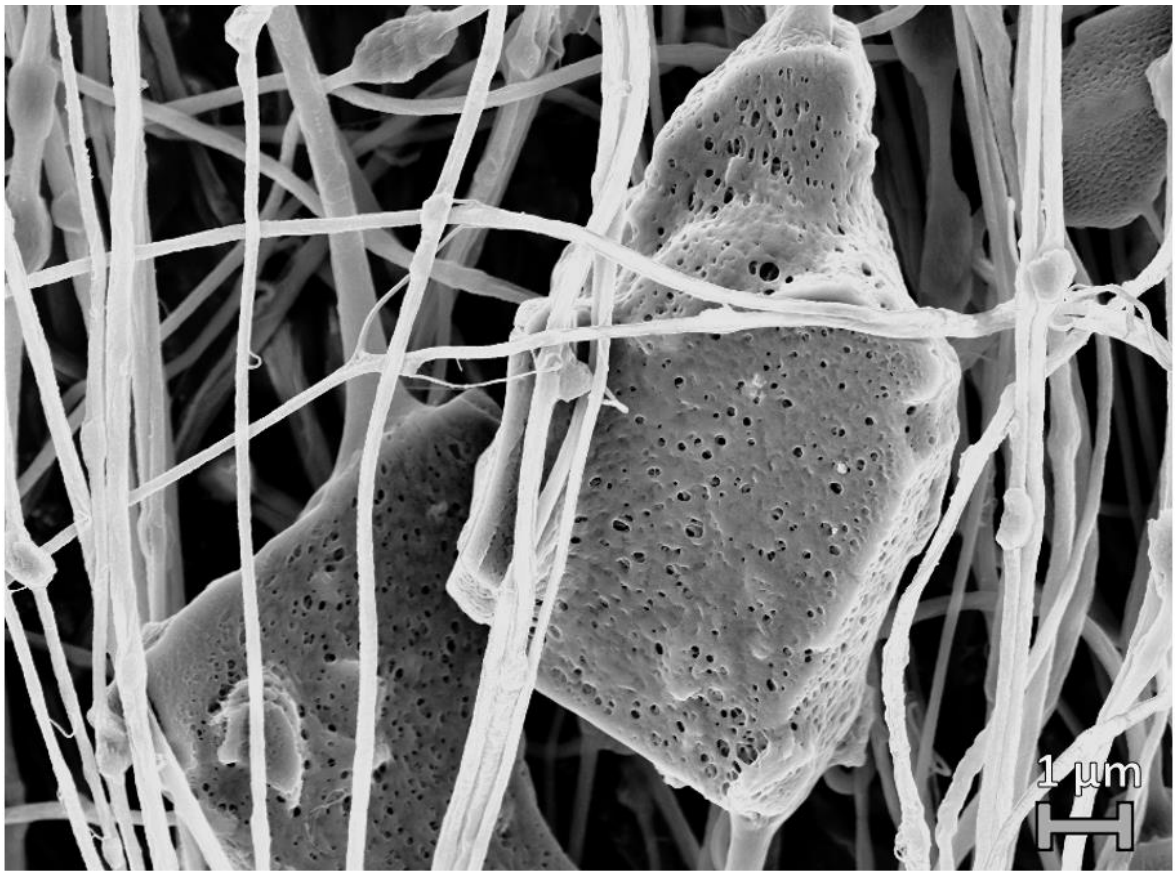

Figure 3.10. SEM image of the SAN+IL+TiC M1 membrane electrospun from 15 wt% SAN in DMF/DCE 70:30 + $EMImBF_4$ + CDC-TiC dispersion prepared via method 1, the scale bar corresponds to 1 µm

With CDC+CB blend containing membranes (SiC+CB and TiC+CB) there was a slight increase in the average fiber diameter when compared to SAN+IL+SiC and SAN+IL+TiC membranes, 14% and 26%, respectively (Figure 3.8). This can be again explained with the higher viscosity of the CB-containing dispersions, although their conductivity is also a little higher. However, the increased diameter might be also caused physically by carbon black particles which have a maximum diameter of 100 nm (Figure 3.11). As they are considerably smaller in size than CDC particles, they can be more easily positioned inside the fibers in a quite uniform way, increasing the average fiber diameter.

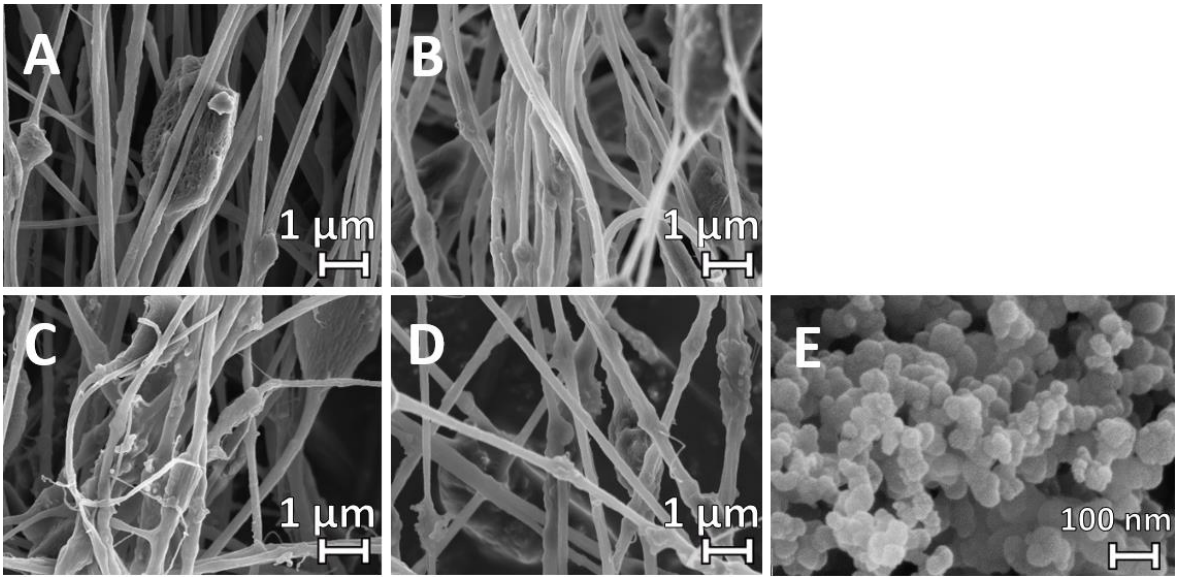

Figure 3.11. SEM images of membranes prepared with method 2: A – SAN+IL+TiC, B – SAN+IL+SiC, C – TiC+CB, D – SiC+CB, the scale bar corresponds to 1 µm. E – SEM image of the carbon black particles, the scale bar corresponds to 100 nm

3.3.2 Mechanical properties

From the 11 electrospun membranes only 8 were mechanically strong enough to be removed from the aluminium foil. The other 3 were membranes which did not contain any ionic liquid (SAN, SAN+TiC, and SAN+SiC), indicating that the addition of ionic liquid to the solution greatly increased the mechanical strength of membranes. Very low tensile strength (0,18 MPa) has been also previously reported for electrospun pure SAN membranes [43], in which case similarly the addition of an ionic liquid increased the tensile strength by 60 times. The author attributed the better mechanical properties to the decrease in the fiber diameter. The decreased fiber diameter has

been shown by several studies to result in a higher molecular chain orientation along the fiber, and the higher chain orientation in turn results in improved tensile strength [82, 83].

However, quite oppositely, the IL-containing membranes in this work have much larger fiber diameters than for example the pure SAN membrane. Therefore some other explanation should be found for this phenomenon. The mechanical strength of electrospun fibers and membranes also depend on the presence of defects (e.g. solvent beads or poorly dispersed carbon agglomerates which may also serve as stress concentrators), the porosity of the fibers, and the alignment of fibers [84-86]. As the addition of ionic liquid reduced the presence of solvent beads, resulted in more homogeneous dispersion of CDCs and increased the uniaxial orientation of SAN fibers (Figures 3.7 and 3.9), the increase in tensile strength seems reasonable, even though the IL-containing fibers are thicker.

Although the 3 IL not containing membranes could not be mechanically tested, the 8 IL-containing electrospun membranes were completely free-standing and possessed extremely good flexibility. Furthermore, they could be easily folded or twisted without inducing any visual damage (Figure 3.12). This combination of flexibility, folding and twisting possibility is very uncommon for supercapacitor electrodes and only a couple of such electrodes have been reported in scientific literature.

Figure 3.12. Bending, folding and twisting operations performed on SAN + IL + SiC method 2 membrane. The last photo was taken of the same sample after performing these operations, the scale bar corresponds to 5 cm on the last photo, thickness of the membrane was 40 µm

The SAN+IL membranes had the highest mechanical strength of all the membranes (Figure 3.13), the addition of CDC-TiC or CDC-SiC reduced the tensile stress by approximately 38% compared to pure SAN+IL membranes. The use of CDC+CB blends in membranes instead of CDC, reduced the tensile stress further and the difference in mechanical strength of SAN+IL and SiC+CB membranes was already 76% (Figure 3.14). This could be attributed to carbon black agglomerates and worse dispersions obtained with CDC+CB, when compared to SAN+IL+CDC dispersions. The agglomerates can act like defects, reducing the mechanical strength of the fibers [85].

From the tensile test results, it can be also concluded that the addition of CDC-TiC reduces the mechanical strength of the membranes less than the addition of CDC-SiC. The same tendency can be seen both with pure CDC and with CDC+CB blend membranes. This can be again due to the better dispersions obtained with CDC-TiC, when compared to CDC-SiC [87].

When comparing the mechanical properties of method 1 and method 2 membranes, then in the case of SAN+IL membranes the M1 membrane has a bit higher mechanical strength than the M2 membrane (Figure 3.13). Although the difference is only 6%, it is intriguing because fibers in M2 membrane are almost twice as thick as M1 fibers. Many studies have also noted that the tensile strength of electrospun fibers increased when the fiber diameter decreased due to the higher orientation of macromolecular chains in thinner fibers [82, 83]. At the same time, the fibers itself were more uniaxially aligned and the solvent beads were completely eliminated in SAN+IL M2 membrane. The higher amount of solvent beads and less aligned fibers of SAN+IL M1 membrane might be also the reason why their difference in tensile stress is so marginal.

Although the membranes were very flexible and with quite good tensile strength in most cases, it should be noted, that due to the highly aligned fibers it was relatively easy to tear the membranes in the alignment direction.

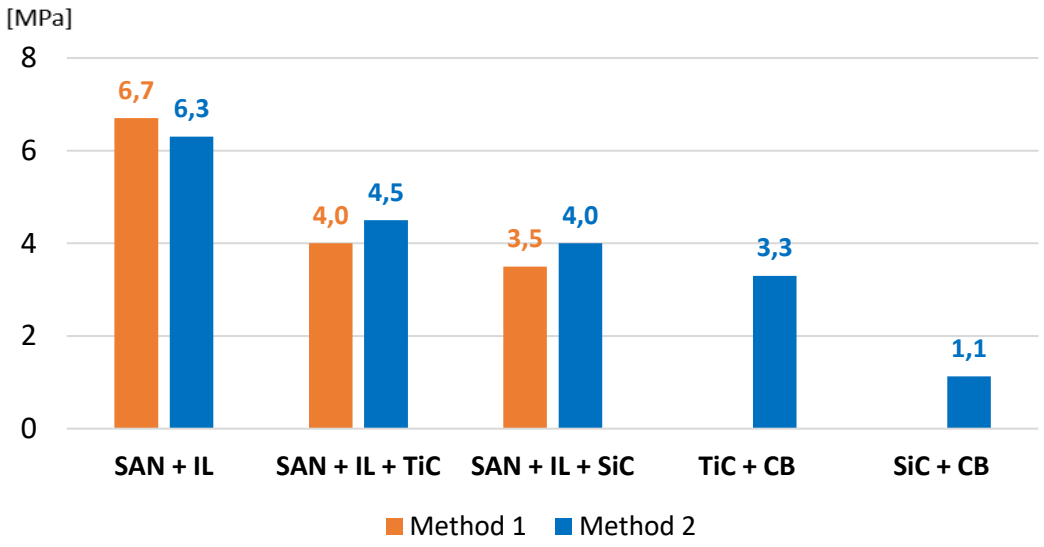

Figure 3.13. Tensile stress values at maximum load for 8 membranes in MPa

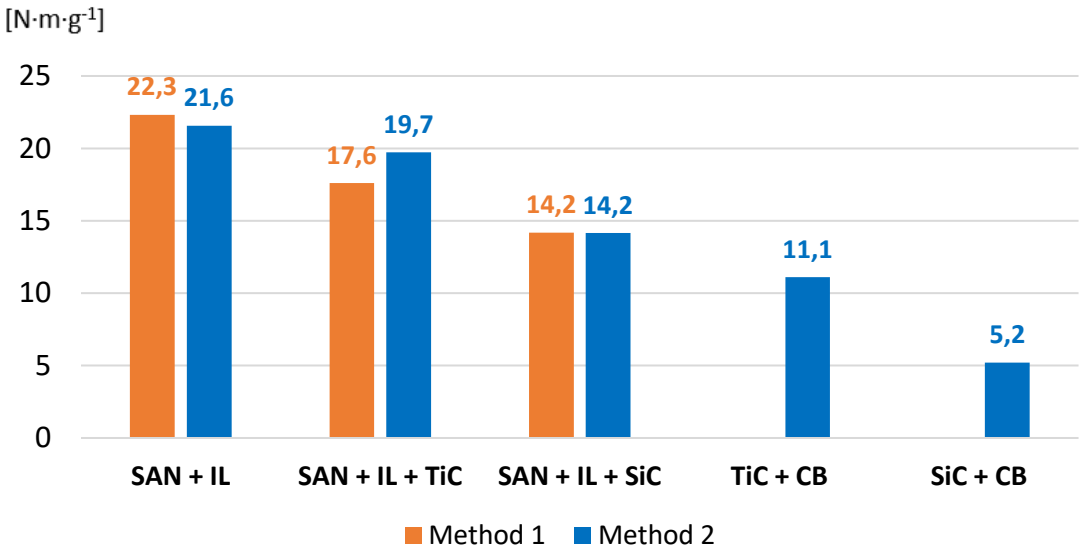

Figure 3.14. Specific stress values at maximum load for 8 membranes in N·m·g^{-1}

3.3.3 Electric conductivity

The electric conductivities of membranes (Figure 3.15) follow roughly the same trend as the electric conductivities of corresponding solutions and dispersions (Figure 3.3). The SAN+IL membranes have the highest conductivity. When carbons are added to the membranes, the electric conductivities are decreased more than 75%, similarly to the solution conductivities. The decrease in conductivity results from the absorbance of IL in the pores of carbonous additives, reducing the mobility of IL ions and thus the conductivity of the membrane.

When comparing two dispersion preparation methods with each other, the method 1 membranes have lower conductivities than method 2 membranes, similarly to the electric conductivities of solutions. Membranes containing CDC-SiC have higher conductivities than membranes containing CDC-TiC, and the addition of conductive additive carbon black increases the conductivities of membranes from 4,6 to 7,6 µS·cm^{-1} (Figure 3.15). The same tendencies could be seen with electric conductivities of solutions and dispersions.

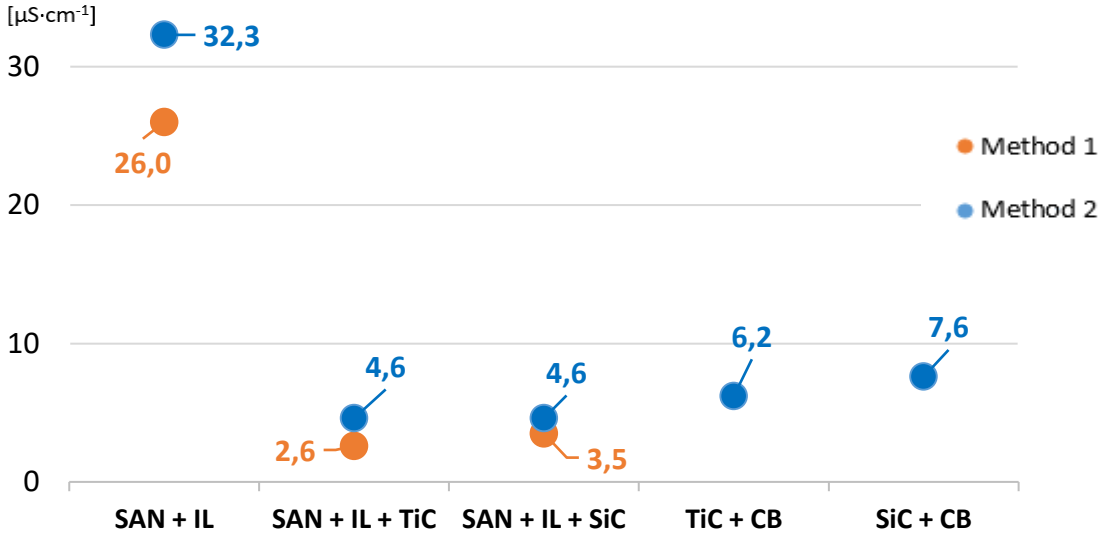

Figure 3.15. Electric conductivities of membranes in µS·cm^{-1}

3.3.4 Capacitance

All the tested membranes have typical EDLC cyclic voltammetry (CV) curves (Figure 3.16). The absence of redox peaks on the CV curves confirm that the capacitance of the membranes in the potential region of 0-1,5 V is only caused by the double-layer capacitance.

The SAN+IL+TiC method 2 membrane had the largest specific capacitance of all the membranes (Figure 3.16), with an integral specific capacitance of 72 F·g^{-1} (Figure 3.17). This could be due to the most suitable porosity, pore size distribution and highest specific surface area of the given membrane [52]. Overall the membranes prepared with method 2 have higher specific capacitances than method 1 membranes, which can be due to the better dispersions and smaller CDC agglomerates obtained with method 2, leading to higher amount of freely accessible pores to the electrolyte and therefore higher effective surface area for the accumulation of the charge [52, 88].

From the measured membranes, the SiC+CB membrane has the lowest specific capacitance (28 F·g^{-1}) (Figure 3.17), which is again explainable with less homogeneous dispersion obtained when compared to pure CDC containing membranes. In addition, as 20 wt% of CDC was substituted with CB and the carbon black has undoubtedly a different surface area and porosity than CDC-SiC, its lower SSA or less suitable pore size could also reduce the specific capacitance. The testing of TiC+CB membrane was not possible, due to its weak resistance to tearing and rupturing during electrode preparation.

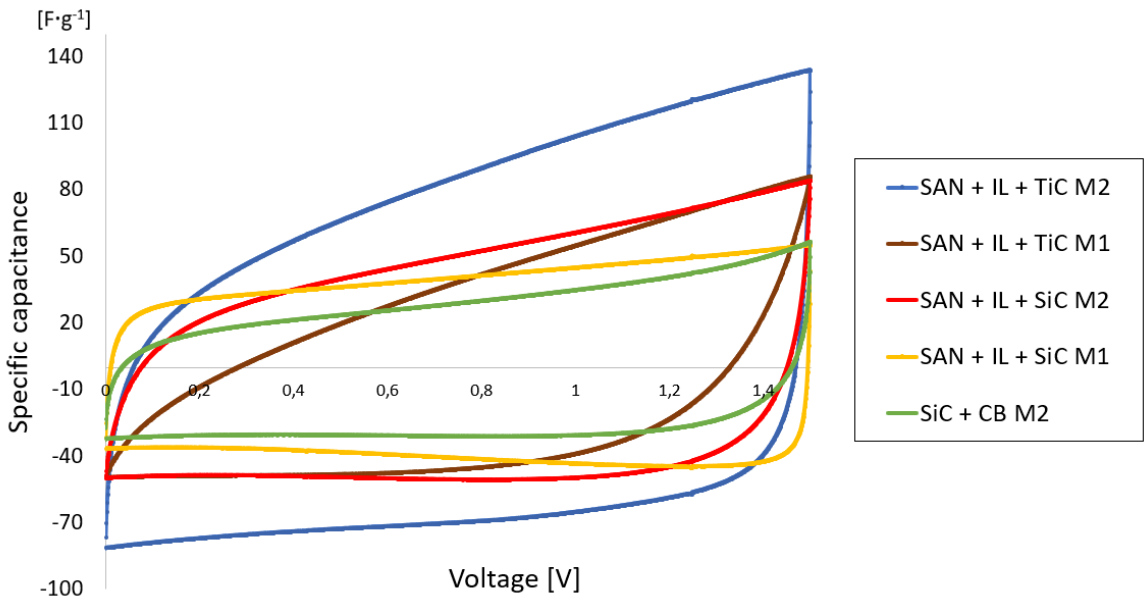

Figure 3.16. Differential specific capacitance [F·g^{-1}] CV curves of membranes, measured at 10 mV·s^{-1} scan rate

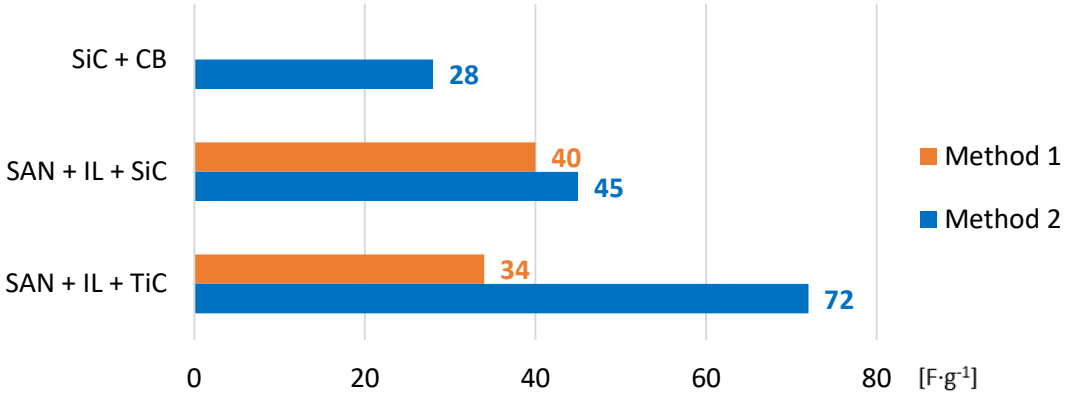

Figure 3.17. Integral specific capacitance values of membranes in F·g^{-1}

The differential and integral specific capacitance curves can be seen in Figure 3.18. The differential specific capacitance curve of SAN+IL+SiC method 1 membrane has the most rectangular shape (Figure 3.18D) and therefore the closest shape to an ideal capacitor. Additionally, the surface areas above and below the x-axis on the CV curve of the same membrane are almost equal (60,1 and 59,5 C·g^{-1}, respectively) in a voltage window of 0 to 1,5 V, meaning that the EDLC can store and give out the same amount of energy, which is desirable. The CV curve's deviation from the rectangular shape depends on several factors, for example on the porous nature of the electrode material and on the resistive behaviour of the material. A higher material resistivity results in the increase of the distortion of the CV curves [89], indicating that the cell prepared with SAN+IL+TiC method 1 membrane might have had the highest internal resistance as its CV curve's shape is the most distorted one (Figure 3.18A).

Quite interestingly, the addition of CB as conductive carbon should reduce the resistivity of the electrode, and therefore reduce the distortion of the CV curve. When comparing the CV curves of SiC+CB M2 and SAN+IL+ SiC M2 membranes, the SiC+CB CV curve does seem a bit more rectangular and the surface areas above and below the x-axis are more equal. However, this difference is quite insignificant, indicating that the cell's resistance is perhaps more influenced by other resistance components, for example by the diffusion resistance of the electrolyte in the pores of the active material [88].

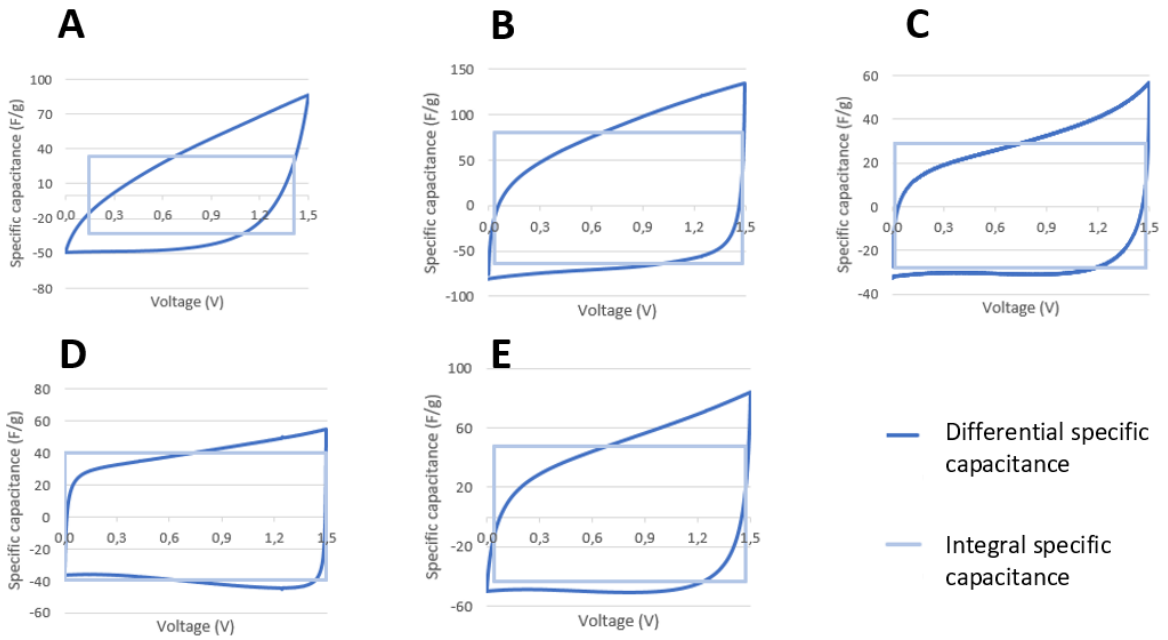

Figure 3.18. Differential vs integral specific capacitance curves of membranes measured at 10 mV·s^{-1} scan rate. A – SAN+IL+TiC M1, B – SAN+IL+TiC M2, C – SiC+CB M2, D – SAN+IL+SiC M1, E – SAN+IL+SiC M2

3.3.5 Porosity and specific surface area

On the basis of the specific capacitance results, two membranes were chosen for BET analysis: the membrane with the highest specific capacitance, and the membrane with the most rectangular shape.

Although the volume of both total porosity and micropores is higher in the case of SAN+IL+SiC method 1 membrane, its specific surface area is lower than that of the SAN+IL+TiC method 2 membrane (Table 3.2). The higher surface area of CDC-TiC containing membrane might be because of its smaller fiber diameter (161 nm vs 188 nm), and due to the rougher surface of fibers when

compared to the CDC-SiC containing membrane (Figure 3.19). The larger specific surface area of SAN+IL+TiC membrane can also explain its higher specific capacitance, but the latter could be also potentially due to a more suitable pore size distribution. Unfortunately, the density functional theory (DFT) method [47] was not used to study the micropore size distribution in this work.

When comparing the porosity of membranes to that of pure CDCs, there is a strong decrease in pore volume (approximately 75%). However, when considering that the membranes contained 50 wt% of SAN and 50 wt% of CDC during the BET analysis, then the decrease in porosity per weight of CDC contained in membranes is a bit less abrupt (49%), but still significant, indicating that the polymer also blocked some of CDC pores and therefore made them inaccessible for N_2 absorption. This decrease in porosity and specific surface area resulted also in the decrease of electrochemical double layer capacitance of CDC contained in membranes compared to pure CDC (72 $F \cdot g^{-1}$ with SAN+IL+TiC M2 membrane vs the maximum obtained capacitance 152 $F \cdot g^{-1}$ in organic electrolyte with CDC-TiC in literature [19]). The decrease in specific surface area (58%) and in maximum specific capacitance (52%), both calculated per CDC-TiC weight, cohere quite well. From these results it can be easily deduced that to increase the capacitance of these membranes, the SSA must be increased, for example by reducing the blocking of CDC pores with the polymer and by increasing the porosity of SAN fibers. Both could be potentially achieved by changing the solvents, solution concentrations or the ionic liquid.

Table 3.2. The specific surface area and pore volume *V* [cm^3] per weight [g] of membrane

Membrane name	BET SSA [$m^2 \cdot g^{-1}$]	*V* (micropores) [$cm^3 \cdot g^{-1}$]	*V* (total porosity) [$cm^3 \cdot g^{-1}$]
SAN+IL+SiC M1	247	0,06	0,22
SAN+IL+TiC M2	333	0,06	0,19

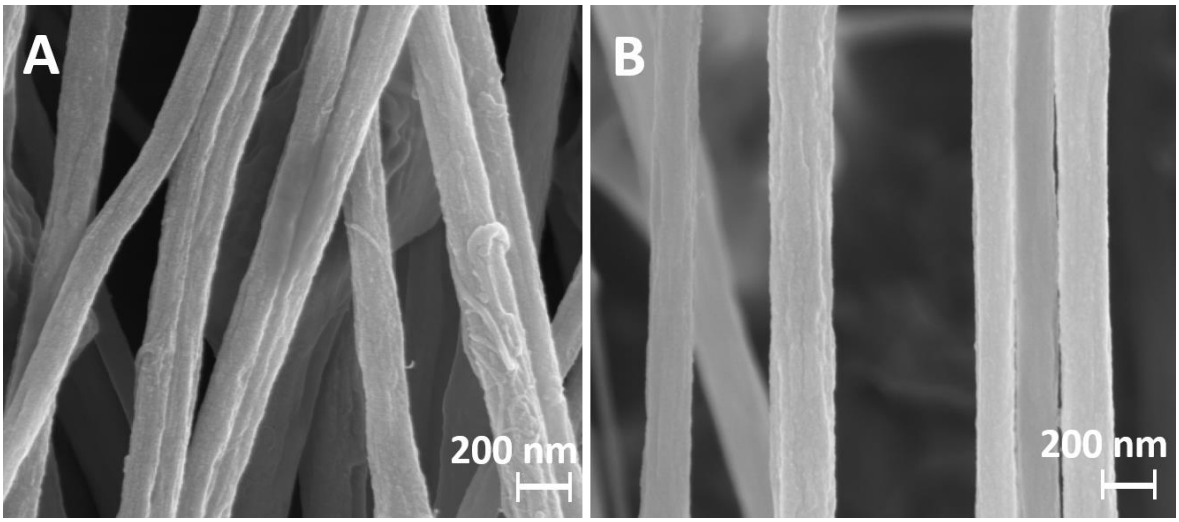

Figure 3.19. SEM images of A – SAN+IL+TiC M2, and B – SAN+IL+SiC M1 membranes demonstrating different fiber surface roughness. The scale bar corresponds to 200 nm

3.3.6 Comparison with flexible supercapacitor electrodes from literature

When comparing the best specific capacitance result obtained from this work (72 $F \cdot g^{-1}$) to the flexible EDLC electrodes from literature (Table 3.3), the obtained result is close to the other reported results, when considering the difference from used electrolytes (specific capacitance in aqueous electrolyte is higher than in organic electrolyte). However, only very few EDLC electrodes were reported in literature which in addition to bending, could be also folded and twisted, similarly to the membranes prepared in this work. When compared to the other twistable electrodes, the electrode in this work had the lowest specific capacitance of these, however, as mentioned in previous chapter, it could be potentially increased for example by reducing the polymer concentration and increasing the CDC concentration, or by using different solvents instead of DMF/DCE solvents mixture to increase the porosity of SAN fibers.

Table 3.3. Prepared flexible supercapacitor electrodes and their specific capacitances from literature

Used carbon and electrode preparation	Specific capacitance [$F \cdot g^{-1}$], in electrolyte type	Foldable and twistable	Reference
Graphene hydrogel thin films	186 in gel	–	[90]
Graphene and cellulose paper composite membranes	120 in gel	–	[4]
Graphene sheets and cotton cloth composite membrane through simple coating and drying process	81,7 in aqueous	–	[91]
Reduced graphene oxide network membranes	81 in gel	–	[92]
CNT coated office papers by drop-dry method	135 in gel	–	[93]
Activated carbon coated cotton and polyester textiles	85 in aqueous	–	[94]
Bamboo-inspired carbon nanofibers by PAN carbonisation	236 in gel	yes	[95]
Activated carbon nanosheet based electrodes by direct spinning, followed by spray coating and subsequent acid treatment	128 in aqueous	yes	[96]
CDC-TiC nanofelt membranes produced by electrospinning, followed by chlorination	120 in organic	–	[40]
PAN-CDC-carbon black composite membranes produced by electrospinning	89 in organic	yes	[97]
SAN-CDC composite membranes produced by electrospinning	72 in organic	yes	Best result from this work

4 SUMMARY

In this work novel fully electrospun, free-standing and flexible supercapacitor electrodes were developed. The prepared electrodes were nanofibrous composite membranes of poly(styrene-co-acrylonitrile) and carbide-derived carbon that could be bent, folded and twisted without any visual damage, and in addition possessed high specific capacitance and sufficient tensile strength. The prepared electrospinning solutions and dispersions and electrospun membranes were characterised by different methods. Solution and dispersion properties such as rheology and conductivity, and membrane properties including morphology, conductivity, porosity, specific surface area, tensile strength and specific capacitance were determined. These results were analysed to find the correlations between the different properties. Finally, the produced electrodes were compared to other flexible supercapacitor electrodes described in scientific literature.

Based on the results the following conclusions can be drawn:

- The 1-hour grinding of CDC particles reduced their average size, but more so with CDC-SiC than CDC-TiC. In both cases the milling decreased the specific surface area, 15% and 3,5%, respectively.
- The addition of ionic liquid $EMImBF_4$ to the polymer solutions and dispersions increased the electric conductivity of the solutions by three orders of magnitude.
- The addition of CDC to IL-containing solutions decreased the solution conductivity because carbonous additives absorbed some of the ionic liquid and solvent. The substitution of 20% of CDC with the conductive additive carbon black increased the solution conductivity only by a few percent.
- Pure $EMImBF_4$ and all the solutions and dispersions had a shear-thinning behaviour, while CB-containing dispersions had unique 3-region behaviour (shear thinning – shear thickening – shear thinning).
- The addition of ionic liquid reduced the shear viscosity of dispersions at higher shear rates due to helping disintegrate the agglomerates into smaller aggregates and acting as a lubricant.
- Overall, method 2 dispersions, where DCE solvent was added before ultrasonication, had lower viscosity values than method 1 dispersions, where DCE was added together with IL as the last component to the dispersion. This indicates that better dispersions were obtained with method 2, owing to the higher amount of solvent per the amount of carbon during ultrasonication.

- All the electrospun membranes consisted of very thin fibers with around 200 nm diameters, an exception was SAN+IL method 2 membrane where the fiber diameter was more than 500 nm. The fibers were highly aligned in the membranes. The CDC and CB particles were inside the fibers, not between them. In places where the polymer coated larger CDC particles, many small pores could be observed in the fiber surface from SEM images.
- Membranes which contained ionic liquid were highly flexible, bendable, foldable and twistable without inducing any visual damage. The addition of carbons decreased the tensile strength of the membranes, especially when CB was added. The highest tensile stress at maximum load for CDC-containing membrane was 4,5 MPa.
- Electric conductivities of the membranes followed the same trends as solution conductivities, 7,6 $\mu S \cdot cm^{-1}$ was the highest conductivity obtained for carbon-containing membranes.
- All the carbon-containing membranes had typical EDLC CV curves and the highest specific capacitance was obtained for SAN+IL+TiC method 2 membrane (72 $F \cdot g^{-1}$).
- Overall, the best specific capacitance result obtained is comparable to the capacitance results of other flexible electrodes reported in scientific literature, but their exact comparison is difficult due to the different electrolytes used in the measurements. However, only very few of these flexible electrodes were also foldable and twistable similarly to the membranes obtained in this work, rendering these properties of EDLC electrodes quite unique. When compared to other twistable electrodes, the best specific capacitance result obtained in this work was a bit lower.
- The electrochemical performance of the developed membranes could be potentially improved by modifying the solution components, e.g. decreasing the polymer concentration and increasing CDC concentration, or using different solvents to obtain SAN fibers with higher porosity for increased specific surface area of the electrodes. For better comparability with other EDLC electrodes reported in literature, the membranes should be tested in also aqueous and/or gel electrolytes.

In conclusion, a novel SAN+CDC composite membrane was developed with unique flexibility and twistability properties and with high specific capacitance. After some further improvement these membranes could be potentially used as supercapacitor electrodes in wearable and portable electronics.

5 LIST OF REFERENCES

[1] L. L. Zhang and X. Zhao, "Carbon-based materials as supercapacitor electrodes," *Chemical Society Reviews,* vol. 38, pp. 2520-2531, 2009.

[2] X. Wang, Y. Li, F. Lou, M. E. M. Buan, E. Sheridan, and D. Chen, "Enhancing capacitance of supercapacitor with both organic electrolyte and ionic liquid electrolyte on a biomass-derived carbon," *RSC Advances,* vol. 7, pp. 23859-23865, 2017.

[3] V. V. Obreja, "Supercapacitors specialities-Materials review," in *AIP Conference Proceedings*, 2014, pp. 98-120.

[4] Z. Weng, Y. Su, D. W. Wang, F. Li, J. Du, and H. M. Cheng, "Graphene–cellulose paper flexible supercapacitors," *Advanced Energy Materials,* vol. 1, pp. 917-922, 2011.

[5] Q. Xue, J. Sun, Y. Huang, M. Zhu, Z. Pei, H. Li*, et al.*, "Recent progress on flexible and wearable supercapacitors," *Small,* vol. 13, 2017.

[6] K. Tõnurist, I. Vaas, T. Thomberg, A. Jänes, H. Kurig, T. Romann*, et al.*, "Application of multistep electrospinning method for preparation of electrical double-layer capacitor half-cells," *Electrochimica Acta,* vol. 119, pp. 72-77, 2014.

[7] X. Luo, J. Wang, M. Dooner, and J. Clarke, "Overview of current development in electrical energy storage technologies and the application potential in power system operation," *Applied Energy,* vol. 137, pp. 511-536, 2015.

[8] A. Pandolfo and A. Hollenkamp, "Carbon properties and their role in supercapacitors," *Journal of power sources,* vol. 157, pp. 11-27, 2006.

[9] R. Kötz and M. Carlen, "Principles and applications of electrochemical capacitors," *Electrochimica acta,* vol. 45, pp. 2483-2498, 2000.

[10] A. Burke, "Ultracapacitors: why, how, and where is the technology," *Journal of power sources,* vol. 91, pp. 37-50, 2000.

[11] E. Kowsari, "High-performance supercapacitors based on ionic liquids and a graphene nanostructure," in *Ionic Liquids-Current State of the Art*, ed: InTech, 2015.

[12] K. Wei and I. S. Kim, "Application of Nanofibers in Supercapacitors," in *Electrospun Nanofibers for Energy and Environmental Applications*, ed: Springer, 2014, pp. 163-181.

[13] B. K. Kim, S. Sy, A. Yu, and J. Zhang, "Electrochemical supercapacitors for energy storage and conversion," *Handbook of Clean Energy Systems,* 2015.

[14] M. D. Stoller and R. S. Ruoff, "Best practice methods for determining an electrode material's performance for ultracapacitors," *Energy & Environmental Science,* vol. 3, pp. 1294-1301, 2010.

[15] M. S. Halper and J. C. Ellenbogen, "Supercapacitors: A brief overview," *The MITRE Corporation, McLean, Virginia, USA,* pp. 1-34, 2006.

[16] P. Simon and Y. Gogotsi, "Materials for electrochemical capacitors," *Nature materials,* vol. 7, p. 845, 2008.

[17] C. Largeot, C. Portet, J. Chmiola, P.-L. Taberna, Y. Gogotsi, and P. Simon, "Relation between the ion size and pore size for an electric double-layer capacitor," *Journal of the American Chemical Society,* vol. 130, pp. 2730-2731, 2008.

[18] M. Arulepp, L. Permann, J. Leis, A. Perkson, K. Rumma, A. Jänes*, et al.*, "Influence of the solvent properties on the characteristics of a double layer capacitor," *Journal of Power Sources,* vol. 133, pp. 320-328, 2004.

[19] I. G. Gogotsi, *Nanomaterials handbook*, 2 ed.: Taylor & Francis Group, 2017.

[20] M. Käärik, M. Arulepp, M. Kook, U. Mäeorg, J. Kozlova, V. Sammelselg*, et al.*, "Characterisation of steam-treated nanoporous carbide-derived carbon of TiC origin: structure and enhanced electrochemical performance," *Journal of Porous Materials,* pp. 1-14.

[21] Q. Huang, D. Wang, and Z. Zheng, "Textile-Based Electrochemical Energy Storage Devices," *Advanced Energy Materials,* vol. 6, 2016.

[22] X. Wang and B. S. Hsiao, "Electrospun nanofiber membranes," *Current opinion in chemical engineering,* vol. 12, pp. 62-81, 2016.

[23] S. Chaudhari, Y. Sharma, P. S. Archana, R. Jose, S. Ramakrishna, S. Mhaisalkar*, et al.*, "Electrospun polyaniline nanofibers web electrodes for supercapacitors," *Journal of Applied Polymer Science,* vol. 129, pp. 1660-1668, 2013.

[24] W. E. Teo and S. Ramakrishna, "A review on electrospinning design and nanofibre assemblies," *Nanotechnology,* vol. 17, p. R89, 2006.

[25] A. Luzio, E. V. Canesi, C. Bertarelli, and M. Caironi, "Electrospun polymer fibers for electronic applications," *Materials,* vol. 7, pp. 906-947, 2014.

[26] D. H. Reneker and A. L. Yarin, "Electrospinning jets and polymer nanofibers," *Polymer,* vol. 49, pp. 2387-2425, 2008.

[27] Z.-M. Huang, Y.-Z. Zhang, M. Kotaki, and S. Ramakrishna, "A review on polymer nanofibers by electrospinning and their applications in nanocomposites," *Composites science and technology,* vol. 63, pp. 2223-2253, 2003.

[28] X. Shi, W. Zhou, D. Ma, Q. Ma, D. Bridges, Y. Ma*, et al.*, "Electrospinning of nanofibers and their applications for energy devices," *Journal of Nanomaterials,* vol. 16, p. 122, 2015.

[29] J. Miao, M. Miyauchi, T. J. Simmons, J. S. Dordick, and R. J. Linhardt, "Electrospinning of nanomaterials and applications in electronic components and devices," *Journal of nanoscience and nanotechnology,* vol. 10, pp. 5507-5519, 2010.

[30] T. Senthil, G. George, and S. Anandhan, "Chemical-resistant ultrafine poly (styrene-co-acrylonitrile) fibers by electrospinning: process optimization by design of experiment," *Polymer-Plastics Technology and Engineering,* vol. 52, pp. 407-421, 2013.

[31] N. Bhardwaj and S. C. Kundu, "Electrospinning: a fascinating fiber fabrication technique," *Biotechnology advances,* vol. 28, pp. 325-347, 2010.

[32] V. Vassiljeva, "Electrospinning of a Polymer Membrane Reinforced with Carbon Nanotubes," PhD Thesis
Tallinn University of Technology, 2018.

[33] J. M. Seo, G. K. Arumugam, S. Khan, and P. A. Heiden, "Comparison of the effects of an ionic liquid and triethylbenzylammonium chloride on the properties of electrospun fibers, 1–poly (lactic acid)," *Macromolecular Materials and Engineering,* vol. 294, pp. 35-44, 2009.

[34] W. Cheng, Q. Yu, Z. Qiu, and Y. Yan, "Effects of different ionic liquids on the electrospinning of a polyacrylonitrile polymer solution," *Journal of Applied Polymer Science,* vol. 130, pp. 2359-2368, 2013.

[35] A. Haider, S. Haider, and I.-K. Kang, "A comprehensive review summarizing the effect of electrospinning parameters and potential applications of nanofibers in biomedical and biotechnology," *Arabian Journal of Chemistry,* 2015.

[36] T. Jarusuwannapoom, W. Hongrojjanawiwat, S. Jitjaicham, L. Wannatong, M. Nithitanakul, C. Pattamaprom*, et al.*, "Effect of solvents on electro-spinnability of polystyrene solutions and morphological appearance of resulting electrospun polystyrene fibers," *European Polymer Journal,* vol. 41, pp. 409-421, 2005.

[37] J. H. Wendorff, S. Agarwal, and A. Greiner, *Electrospinning: materials, processing, and applications*: John Wiley & Sons, 2012.

[38] P. Heikkilä and A. Harlin, "Electrospinning of polyacrylonitrile (PAN) solution: Effect of conductive additive and filler on the process," *Express Polymer Letters,* vol. 3, pp. 437-445, 2009.

[39] L. Coustan and F. Favier, "5 Electrospun Nanofibers for Supercapacitors," *Electrospinning for Advanced Energy and Environmental Applications,* p. 107, 2015.

[40] Y. Gao, V. Presser, L. Zhang, J. J. Niu, J. K. McDonough, C. R. Pérez*, et al.*, "High power supercapacitor electrodes based on flexible TiC-CDC nano-felts," *Journal of Power Sources,* vol. 201, pp. 368-375, 2012.
[41] C. A. Harper, *Modern Plastics Handbook: Handbook*: McGraw-Hill Professional, 2000.
[42] T. Senthil and S. Anandhan, "Fabrication of styrene–acrylonitrile random copolymer nanofiber membranes from N, N-dimethyl formamide by electrospinning," *Journal of Elastomers & Plastics,* vol. 47, pp. 327-346, 2015.
[43] V. Vassiljeva, K.-K. Kirikal, S. Hietala, T. Kaljuvee, V. Mikli, M. Rähn*, et al.*, "One-step carbon nanotubes grafting with styrene-co-acrylonitrile by reactive melt blending for electrospinning of conductive reinforced composite membranes," *Fullerenes, Nanotubes and Carbon Nanostructures,* vol. 25, pp. 667-677, 2017.
[44] Sigma-Aldrich, "Product Specification Sheet of Poly(Styrene-co-Acrylonitrile)."
[45] V. Gudkova, A. Krumme, T. Märtson, M. Rikko, E. Tarassova, and M. Viirsalu, "The impact of 1-butyl-3-methylimidazolium chloride on electrospinning process of SAN polymer solutions and electrospun fiber morphology," *Journal of Electrostatics,* vol. 72, pp. 433-436, 2014.
[46] Y. Zhao, W. Wang, D.-B. Xiong, G. Shao, W. Xia, S. Yu*, et al.*, "Titanium carbide derived nanoporous carbon for supercapacitor applications," *international journal of hydrogen energy,* vol. 37, pp. 19395-19400, 2012.
[47] J. Leis, M. Arulepp, A. Kuura, M. Lätt, and E. Lust, "Electrical double-layer characteristics of novel carbide-derived carbon materials," *Carbon,* vol. 44, pp. 2122-2129, 2006.
[48] J. Fernandez, M. Arulepp, J. Leis, F. Stoeckli, and T. A. Centeno, "EDLC performance of carbide-derived carbons in aprotic and acidic electrolytes," *Electrochimica Acta,* vol. 53, pp. 7111-7116, 2008.
[49] Sigma-Aldrich. (14.05.2018). *Carbides - pricing*. Available: https://www.sigmaaldrich.com/materials-science/material-science-products.html?TablePage=19295138
[50] M. Youssry, L. Madec, P. Soudan, M. Cerbelaud, D. Guyomard, and B. Lestriez, "Non-aqueous carbon black suspensions for lithium-based redox flow batteries: rheology and simultaneous rheo-electrical behavior," *Physical Chemistry Chemical Physics,* vol. 15, pp. 14476-14486, 2013.
[51] C. Schütter, C. Ramirez-Castro, M. Oljaca, S. Passerini, M. Winter, and A. Balducci, "Activated carbon, carbon blacks and graphene based nanoplatelets as active materials for electrochemical double layer capacitors: a comparative study," *Journal of The Electrochemical Society,* vol. 162, pp. A44-A51, 2015.
[52] J. S. Moon, H. Kim, D.-C. Lee, J. T. Lee, and G. Yushin, "Increasing capacitance of zeolite-templated carbons in electric double layer capacitors," *Journal of The Electrochemical Society,* vol. 162, pp. A5070-A5076, 2015.
[53] R. Peng, Y. Wang, W. Tang, Y. Yang, and X. Xie, "Progress in imidazolium ionic liquids assisted fabrication of carbon nanotube and graphene polymer composites," *Polymers,* vol. 5, pp. 847-872, 2013.
[54] T. L. Greaves and C. J. Drummond, "Protic Ionic Liquids: Properties and Applications," *Chemical Reviews,* vol. 108, pp. 206-237, 2008/01/01 2008.
[55] H. Weingärtner, "Understanding ionic liquids at the molecular level: facts, problems, and controversies," *Angewandte Chemie International Edition,* vol. 47, pp. 654-670, 2008.
[56] S. T. Handy, Ed., *Ionic Liquids - Classes and Properties*. InTechOpen, 2011, p.^pp. Pages.
[57] J. Wang, H. Chu, and Y. Li, "Why Single-Walled Carbon Nanotubes Can Be Dispersed in Imidazolium-Based Ionic Liquids," *ACS Nano,* vol. 2, pp. 2540-2546, 2008/12/23 2008.
[58] Sigma-Aldrich, "Ionic Liquids," *Chemfiles,* vol. 5, 2005.
[59] V. V. Chaban, I. V. Voroshylova, O. N. Kalugin, and O. V. Prezhdo, "Acetonitrile Drastically Boosts Conductivity of Ionic Liquids," *arXiv preprint arXiv:1202.1006,* 2012.

[60] Sigma-Aldrich, "Product specification sheets of ionic liquids from Sigma-Aldrich webpage," 2018.
[61] R. Biczak, B. Pawłowska, P. Bałczewski, and P. Rychter, "The role of the anion in the toxicity of imidazolium ionic liquids," *Journal of hazardous materials,* vol. 274, pp. 181-190, 2014.
[62] D. Zhao, Y. Liao, and Z. Zhang, "Toxicity of ionic liquids," *Clean–soil, air, water,* vol. 35, pp. 42-48, 2007.
[63] E. Brown, N. A. Forman, C. S. Orellana, H. Zhang, B. W. Maynor, D. E. Betts*, et al.*, "Generality of shear thickening in dense suspensions," *Nature materials,* vol. 9, p. 220, 2010.
[64] (28.04.2018). *Basics of rheology*. Available: https://wiki.anton-paar.com/en/basics-of-rheology/#introduction-to-rheology
[65] (28.04.2018). *Basics of viscometry*. Available: https://wiki.anton-paar.com/en/basic-of-viscometry/
[66] (28.04.2018). *Flow curve and yield point determination with rotational viscometry*. Available: https://wiki.anton-paar.com/en/flow-curve-and-yield-point-determination-with-rotational-viscometry/
[67] (28.04.2018). *Internal structures of samples and shear-thinning behavior*. Available: https://wiki.anton-paar.com/en/internal-structures-of-samples-and-shear-thinning-behavior/
[68] A. Metzner, "Rheology of suspensions in polymeric liquids," *Journal of rheology,* vol. 29, pp. 739-775, 1985.
[69] G. L. Burrell, N. F. Dunlop, and F. Separovic, "Non-Newtonian viscous shear thinning in ionic liquids," *Soft Matter,* vol. 6, pp. 2080-2086, 2010.
[70] B. J. Maranzano and N. J. Wagner, "The effects of particle size on reversible shear thickening of concentrated colloidal dispersions," *The Journal of chemical physics,* vol. 114, pp. 10514-10527, 2001.
[71] N. J. Wagner and J. F. Brady, "Shear thickening in colloidal dispersions," *Physics Today,* vol. 62, pp. 27-32, 2009.
[72] S. Shiraishi, "Electrochemical performance," in *Materials science and engineering of carbon: characterization*, M. Inagaki and F. Kang, Eds., ed: Butterworth-Heinemann, 2016.
[73] D. Qu and H. Shi, "Studies of activated carbons used in double-layer capacitors," *Journal of Power Sources,* vol. 74, pp. 99-107, 1998.
[74] P. Yang and W. Mai, "Flexible solid-state electrochemical supercapacitors," *Nano Energy,* vol. 8, pp. 274-290, 2014.
[75] T. Adinaveen, J. J. Vijaya, and L. J. Kennedy, "Comparative Study of Electrical Conductivity on Activated Carbons Prepared from Various Cellulose Materials," *Arabian Journal for Science and Engineering,* vol. 41, pp. 55-65, 2016.
[76] C. Samaras. (2013, 04.05.2018). *Numerical integration in Excel using the trapezoidal rule*. Available: https://www.myengineeringworld.net/2013/06/integration-in-excel-trapezoidal-rule.html
[77] C. L. Zirbel. (2009, 04.05.2018). *Numerical integration of a function known only through data points*. Available: personal.bgsu.edu/~zirbel/5920/calculator/numerical_integration.pdf
[78] B. Dyatkin, O. Gogotsi, B. Malinovskiy, Y. Zozulya, P. Simon, and Y. Gogotsi, "High capacitance of coarse-grained carbide derived carbon electrodes," *Journal of Power Sources,* vol. 306, pp. 32-41, 2016.
[79] Y. Feng, H. Zou, M. Tian, L. Zhang, and J. Mi, "Relationship between dispersion and conductivity of polymer nanocomposites: a molecular dynamics study," *The Journal of Physical Chemistry B,* vol. 116, pp. 13081-13088, 2012.
[80] W. K. Son, J. H. Youk, T. S. Lee, and W. H. Park, "Electrospinning of ultrafine cellulose acetate fibers: studies of a new solvent system and deacetylation of ultrafine cellulose acetate fibers," *Journal of Polymer Science Part B: Polymer Physics,* vol. 42, pp. 5-11, 2004.

[81] S. Ramakrishna, *An introduction to electrospinning and nanofibers*: World Scientific, 2005.
[82] S.-C. Wong, A. Baji, and S. Leng, "Effect of fiber diameter on tensile properties of electrospun poly (ε-caprolactone)," *Polymer,* vol. 49, pp. 4713-4722, 2008.
[83] A. Baji, Y.-W. Mai, S.-C. Wong, M. Abtahi, and P. Chen, "Electrospinning of polymer nanofibers: effects on oriented morphology, structures and tensile properties," *Composites science and technology,* vol. 70, pp. 703-718, 2010.
[84] M. Richard-Lacroix and C. Pellerin, "Molecular orientation in electrospun fibers: from mats to single fibers," *Macromolecules,* vol. 46, pp. 9473-9493, 2013.
[85] B.-X. Yang, J.-H. Shi, K. Pramoda, and S. H. Goh, "Enhancement of stiffness, strength, ductility and toughness of poly (ethylene oxide) using phenoxy-grafted multiwalled carbon nanotubes," *Nanotechnology,* vol. 18, p. 125606, 2007.
[86] J. Yao, C. W. Bastiaansen, and T. Peijs, "High strength and high modulus electrospun nanofibers," *Fibers,* vol. 2, pp. 158-186, 2014.
[87] L. Q. Liu, D. Tasis, M. Prato, and H. D. Wagner, "Tensile mechanics of electrospun multiwalled nanotube/poly (methyl methacrylate) nanofibers," *Advanced Materials,* vol. 19, pp. 1228-1233, 2007.
[88] Y. Suda, A. Mizutani, T. Harigai, H. Takikawa, H. Ue, and Y. Umeda, "Influences of internal resistance and specific surface area of electrode materials on characteristics of electric double layer capacitors," in *AIP Conference Proceedings*, 2017, p. 020022.
[89] A. Allagui, T. J. Freeborn, A. S. Elwakil, and B. J. Maundy, "Reevaluation of performance of electric double-layer capacitors from constant-current charge/discharge and cyclic voltammetry," *Scientific reports,* vol. 6, p. 38568, 2016.
[90] Y. Xu, Z. Lin, X. Huang, Y. Liu, Y. Huang, and X. Duan, "Flexible solid-state supercapacitors based on three-dimensional graphene hydrogel films," *ACS nano,* vol. 7, pp. 4042-4049, 2013.
[91] W.-w. Liu, X.-b. Yan, J.-w. Lang, C. Peng, and Q.-j. Xue, "Flexible and conductive nanocomposite electrode based on graphene sheets and cotton cloth for supercapacitor," *Journal of Materials Chemistry,* vol. 22, pp. 17245-17253, 2012.
[92] T. Purkait, G. Singh, D. Kumar, M. Singh, and R. S. Dey, "High-performance flexible supercapacitors based on electrochemically tailored three-dimensional reduced graphene oxide networks," *Scientific reports,* vol. 8, p. 640, 2018.
[93] Y. J. Kang, H. Chung, C.-H. Han, and W. Kim, "All-solid-state flexible supercapacitors based on papers coated with carbon nanotubes and ionic-liquid-based gel electrolytes," *Nanotechnology,* vol. 23, p. 065401, 2012.
[94] K. Jost, C. R. Perez, J. K. McDonough, V. Presser, M. Heon, G. Dion*, et al.*, "Carbon coated textiles for flexible energy storage," *Energy & Environmental Science,* vol. 4, pp. 5060-5067, 2011.
[95] Y. Sun, R. B. Sills, X. Hu, Z. W. Seh, X. Xiao, H. Xu*, et al.*, "A bamboo-inspired nanostructure design for flexible, foldable, and twistable energy storage devices," *Nano letters,* vol. 15, pp. 3899-3906, 2015.
[96] J. H. Jun, H. Song, C. Kim, I. S. Choi, Y. Jeong, and J. H. Lee, "Carbon-Nanosheet Based Large-Area Electrochemical Capacitor that is Flexible, Foldable, Twistable, and Stretchable," *Small,* p. 1702145, 2018.
[97] N. S. S. Malmberg, M. Käärik, A. Krumme, M. Arulepp, "Producing electrospun composite electrodes for supercapacitors," *Baltic Polymer Symposium Book of Abstracts,* p. 70, 2017.